

**Physics of Radioactive Beams<sup>1</sup>**  
**Chapter 3**  
*Nuclear astrophysics*

Carlos A. Bertulani, Texas A&M University-Commerce, TX 75429, USA

<sup>1</sup>These notes consist of a series of lectures presented by the author at the Gesellschaft für Schwerionenforschung, Darmstadt, Germany in the Spring of 1994. GSI-Report 1994-11. This material was latter extended and published in the book “Physics of Radioactive Beams”, C.A. Bertulani, M. Hussein and G. Muenzenberg, Nova Science, Hauppauge, NY, 2002, ISBN: 1-59033-141-9

## 0.1 Standard stellar evolution

### 0.1.1 Hydrogen and CNO cycles

The energy production in the stars is a well known process. The initial energy which ignites the process arises from the gravitational contraction of a mass of gas. The contraction increases the pressure, temperature, and density, at the center of the star until values able to start the thermonuclear reactions (see Supplement A), initiating the star lifetime. The energy liberated in these reactions yield a pressure in the plasma, which opposes compression due to gravitation. Thus, an equilibrium is reached for the energy which is produced, the energy which is liberated by radiation, the temperature, and the pressure.

The Sun is a star in its initial phase of evolution. The temperature in its surface is  $6000^\circ\text{C}$ , while in its interior the temperature reaches  $1.5 \times 10^7\text{ K}$ , with a pressure given by  $6 \times 10^{11}\text{ atm}$  and density  $150\text{ g/cm}^3$ . The present mass of the Sun is  $M_\odot = 2 \times 10^{33}\text{ g}$  and its main composition is hydrogen (70%), helium (29%) and less than 1% of more heavy elements, like carbon, oxygen, etc.

What are the nuclear processes which originate the huge thermonuclear energy of the Sun, and that has last  $4.6 \times 10^9$  years (the assumed age of the Sun)? It cannot be the simple fusion of two protons, or of  $\alpha$ -particles, or even the fusion of protons with  $\alpha$ -particles, since neither  ${}^2_2\text{He}$ ,  ${}^8_4\text{Be}$ , or  ${}^5_3\text{Li}$ , are not stable. The only possibility is the proton-proton fusion in the form



which occurs via the  $\beta$ -decay, i.e., due to the weak-interaction. The cross section for this reaction for protons of energy around 1 MeV is very small, of the order of  $10^{-23}\text{ b}$ . The average lifetime of protons in the Sun due to the transformation to deuterons by means of Eq. 1 is about  $10^{10}\text{ y}$ . This explains why the energy radiated from the Sun is approximately constant in time, and not by means of an explosive process.

The deuteron produced in the above reaction is consumed almost immediately in the process



The resulting  ${}^3_2\text{He}$  reacts by means of



which produces the stable nucleus  ${}^4_2\text{He}$  with a great energy gain, or by means of the reaction



In the second case, a chain reaction follows as



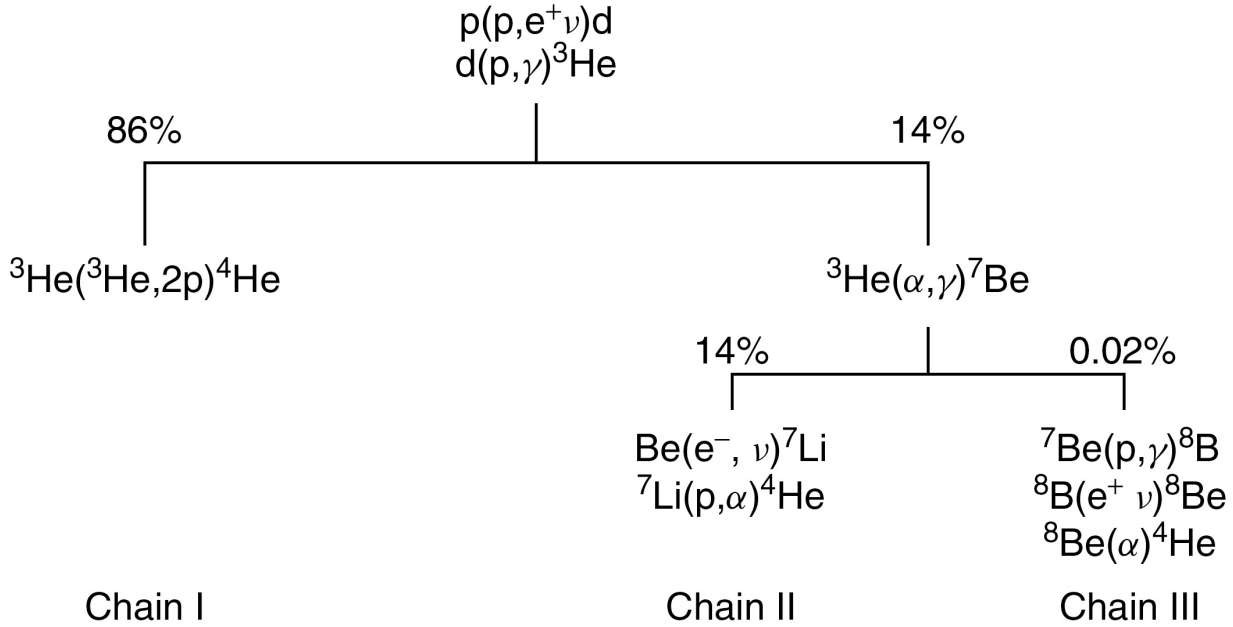


Figure 1: The chain reaction (p-p cycle). The percentage for the several branches are calculated in the center of the sun [1].

or



The chain reaction 1-6 is called the hydrogen cycle. The result of this cycle is the transformation of four protons in an  $\alpha$ -particle, with an energy gain of 26,7 MeV, about 20% of which are carried away by the neutrinos (see Fig. 1).

If the gas which gives birth to the star contains heavier elements, another cycle can occur; the *carbon cycle*, or *CNO cycle*. In this cycle the carbon, oxygen, and nitrogen nuclei are catalyzers of nuclear processes, with the end product also in the form  $4p \longrightarrow {}^4_2\text{He}$ . Fig. 2(a) describes the CNO cycle. Due to the larger Coulomb repulsion between the carbon nuclei, it occurs at higher temperatures (larger relative energy between the participant nuclei), up to  $1.4 \times 10^7$  K. In the Sun the hydrogen cycle prevails. But, in stars with larger temperatures the CNO cycle is more important. Fig. 2(b) compares the energy production in stars for the hydrogen and for the CNO cycle as a function of the temperature at their center. For the Sun temperature,  $T_\odot$ , we see that the pp cycle is more efficient.

After the protons are transformed into helium at the center of a star like our Sun, the fusion reactions start to consume protons at the surface of the star. At this stage the star starts to become a *red giant*. The energy generated by fusion increases the temperature and

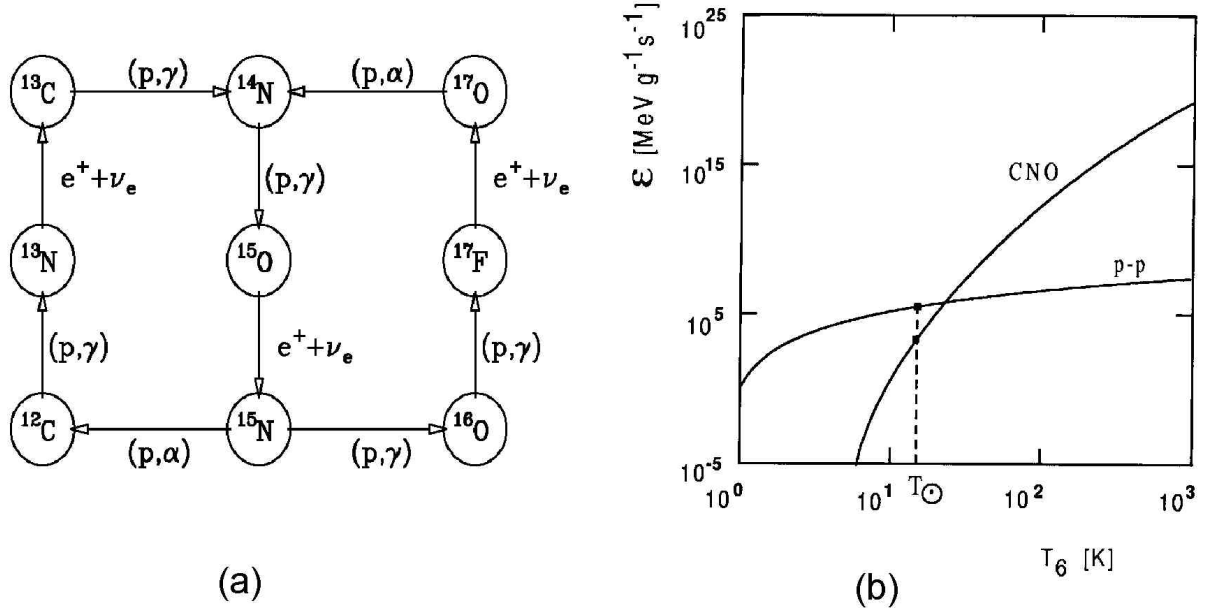
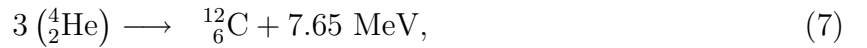


Figure 2: (a) The CNO cycle. (b) Comparison of the energy production in the pp and in the CNO cycle as a function of the star temperature [2].

expands the surface of the star. The star luminosity increases. The red giant contracts again after the hydrogen fuel is burned.

Other thermonuclear processes start. The first is the helium burning when the temperature reaches  $10^8$  K and the density becomes  $10^6$  g.cm $^{-3}$ . Helium burning starts with the triple capture reaction



followed by the formation of oxygen via the reaction



For a star with the Sun mass, helium burning occurs in about  $10^7$  y. For a much heavier star the temperature can reach  $10^9$  K. The compression process followed by the burning of heavier elements can lead to the formation of iron. After that the thermonuclear reactions are no more energetic and the star stops producing nuclear energy.

### 0.1.2 White dwarfs and neutron stars

If the thermonuclear processes in massive stars achieve the production of iron, there are the following possibilities for the star evolution.

(a) For stars with masses  $< 1, 2 M_\odot$  the internal pressure of the degenerated electron gas (i.e., when the electrons occupy all states allowed by the Pauli principle) does not allow the star compression due to the gravitational attraction to continue indefinitely. For a free electron gas at temperature  $T = 0$  (lowest energy state), the electrons occupy all energy states up to the Fermi energy. The total density of the star can be calculated adding up the individual electronic energies. Since each phase-space cell  $d^3p \cdot V$  (where  $V$  is the volume occupied by the electrons) contains  $d^3p \cdot V / (2\pi\hbar)^3$  states, we get

$$\begin{aligned} \frac{E}{V} &= 2 \int_0^{p_F} \frac{d^3p}{(2\pi\hbar)^3} E(p) = 2 \int_0^{p_F} \frac{d^3p}{(2\pi\hbar)^3} \sqrt{p^2c^2 + m_e^2c^4} = n_0 m_e c^2 x^3 \epsilon(x), \\ \epsilon(x) &= \frac{3}{8x^3} \{x(1+2x^2)(1+x^2)^{1/2} - \log[x + (1+x)^{1/2}]\}, \end{aligned} \quad (9)$$

where the factor 2 is due to the electron spin, and

$$x = \frac{p_F c}{m_e c^2} = \left(\frac{n}{n_0}\right)^{1/3} = \left(\frac{\rho}{\rho_0}\right)^{1/3}, \quad (10)$$

where

$$n_0 = \frac{m_e^3 c^3}{\hbar^3} \quad \text{and} \quad \rho_0 = \frac{m_N n_0}{Y_e} = 9,79 \times 10^5 Y_e^{-1} \text{ g/cm}^3. \quad (11)$$

In the above relations  $p_F$  is the Fermi momentum of the electrons,  $m_e$  ( $m_N$ ) is the electron (nucleon) mass,  $n$  is the density of electrons, and  $\rho$  is the mass density in the star.  $Y_e$  is the number of electrons per nucleon.

The variable  $x$  characterizes the electron density in terms of

$$n_0 = 5,89 \times 10^{29} \text{ cm}^{-3}. \quad (12)$$

At this density the Fermi momentum is equal to the inverse of the Compton wavelength of the electron.

Using traditional methods of thermodynamics, the pressure is related to the energy variation by

$$P = -\frac{\partial E}{\partial V} = -\frac{\partial E}{\partial x} \frac{\partial x}{\partial V} = -\frac{\partial E}{\partial x} \left(-\frac{x}{3V}\right) = \frac{1}{3} n_0 m_e c^2 x^4 \frac{d\epsilon}{dx}. \quad (13)$$

This model allows us to calculate the pressure in the electron gas in a very simple form. Since the pressure increases with the electron density, which increases with the decreasing volume of the star, we expect that the gravitational collapse stops when the electronic pressure equals the gravitational pressure. When this occurs the star cools slowly and its luminosity decreases. The star becomes a *white dwarf* and in some cases its diameter can become smaller than that of the Moon.

(b) For stars with masses in the interval 1.2 - 1.6  $M_\odot$ , the electron pressure is not sufficient to balance the gravitational attraction. The density increases to  $2 \times 10^{14} \text{ g.cm}^{-3}$

and the matter "neutronizes". This occurs via the electron capture by the nuclei (inverse beta decay), transforming protons into neutrons. The final product is a *neutron star*, with a small radius. For example, if it were possible to form a neutron star from the Sun it would have a radius given by

$$\left(\frac{M_{\odot}}{\frac{4\pi}{3}\rho}\right)^{1/3} = \left(\frac{2 \times 10^{33} \text{ g}}{\frac{4\pi}{3} \times 2 \times 10^{14} \text{ g cm}^{-3}}\right)^{1/3} \simeq 14 \text{ km.}$$

The process of transformation of iron nuclei into neutron matter occurs as following: for densities of the order of  $1.15 \times 10^9 \text{ g}\cdot\text{cm}^{-3}$  the Fermi energy of the electron gas is larger than the upper energy of the energy spectrum for the  $\beta$ -decay of the isotope  $^{56}_{25}\text{Mn}$ . The decay of this isotope can be inverted and two neutron-rich isotopes of  $^{56}_{25}\text{Mn}$  are formed, i.e.,



These nuclei transform in  $^{56}_{24}\text{Cr}$  by means of the reaction



With the increasing of the pressure more isotopes can be formed, until neutrons start being emitted:



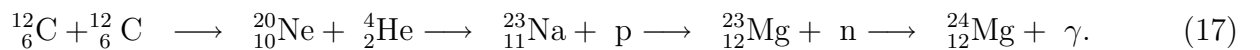
For  $^{56}_{26}\text{Fe}$  this reaction network starts to occur at an energy of 22 MeV, which corresponds to a density of  $4 \times 10^{11} \text{ g}\cdot\text{cm}^{-3}$ . With increasing density, the number of free neutrons increases and, when the density reaches  $2 \times 10^{14} \text{ g}\cdot\text{cm}^{-3}$ , the density of free neutrons is 100 times larger than the density of the remaining electrons.

### 0.1.3 Synthesis of elements

In Figure 3(a) we show the relative distribution of elements in our galaxy. It has two distinct regions: in the region  $A < 100$  it decreases with  $A$  approximately like an exponential, whereas for  $A > 100$  it is approximately constant, except for the peaks in the region of the magic numbers  $Z = 50$  e  $N = 50, 82, 126$ .

The thermonuclear processes 1-8 can explain the relative abundance of  $^4_2\text{He}$ ,  $^{12}_6\text{C}$  and  $^{16}_8\text{O}$ . The processes occurring after  $^4_2\text{He}$  burning mainly form isotopes of  $^{20}_{10}\text{Ne}$ ,  $^{24}_{12}\text{Mg}$  and  $^{28}_{14}\text{Si}$ . We can understand the small abundance of the elements Li, Be and B as due to the small velocity with which they are formed via the reaction 4 and the first equation of 5, while they are rapidly consumed by the second reaction in 5 and the first reaction in 6.

The synthesis of elements heavier than oxygen occur when, after the helium burn, a new compression and heating of the star rises the temperature to values higher than  $6 \times 10^8 \text{ K}$ . This situation ignites an intense carbon burning:



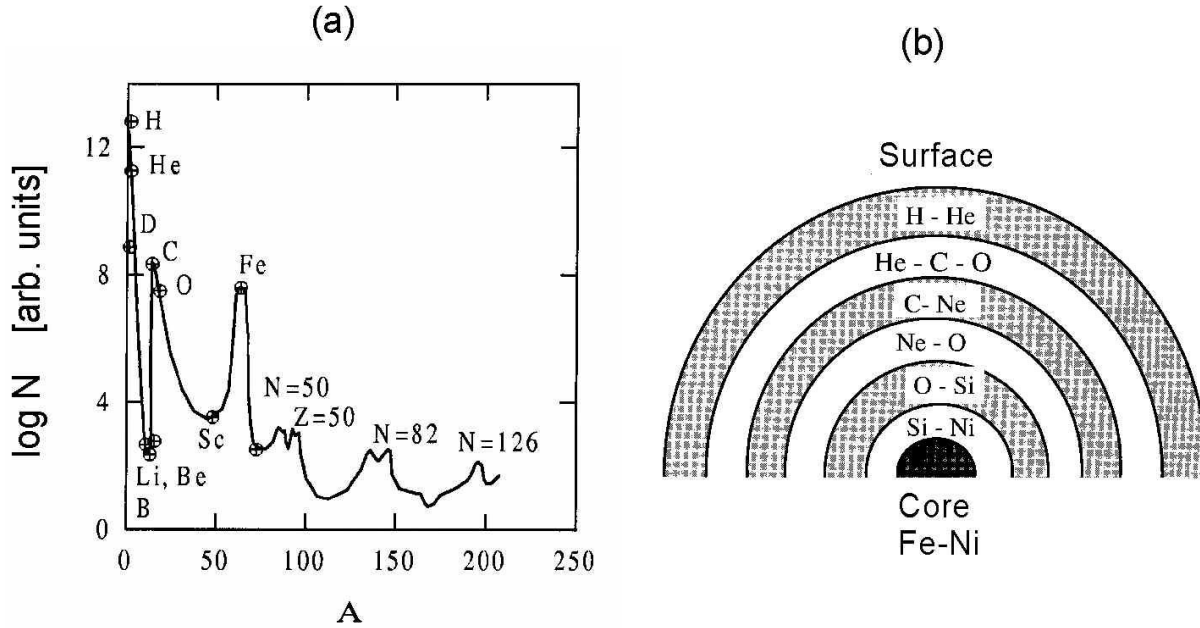


Figure 3: (a) Relative distribution of elements in our galaxy. (b) The “onion” structure of a supernova.

Carbon and oxygen can also burn simultaneously:



For temperatures above  $3 \times 10^9$  K more photo-nuclear processes appear. These yield more nuclei to be burned and heavier nuclei are produced:



Due to the large number of free neutrons, many  $(n, \gamma)$ -reactions (radiative neutron capture) elements in the mass range  $A = 28, \dots, 57$  are formed. This leads to a large abundance of elements in the iron mass region, which have the largest binding energy per nucleon. For elements heavier than iron the nuclear fusion processes do not generate energy.

For  $A > 100$  the distribution of nuclei cannot be explained in terms of fusion reactions with charged particles. They are formed by the successive capture of slow neutrons and of  $\beta^-$ -decay. The maxima of the element distribution in  $N = 50, 82, 126$  are due to the small capture cross sections corresponding to the magic numbers. This yields a trash of isotopes at the observed element distribution.

### 0.1.4 Supernovae explosions

It has long been observed that, occasionally, a new star appears in the sky, increases its brightness to a maximum value, and decays afterwards until its visual disappearance. Such stars were called by *novae*. Among the novae some stars present an exceptional variation in their brightness and are called by *supernovae*.

Schematically a pre-supernova has the onion structure presented in figure 3(b). Starting from the center of the star, we first find a core of iron, the remnant of silicon burning. After that we pass by successive regions where  $^{28}\text{Si}$ ,  $^{16}\text{O}$ ,  $^{12}\text{C}$ ,  $^4\text{He}$ , and  $^1\text{H}$  form the dominant fraction. In the interfaces, the nuclear burning continues to happen.

The silicon burning exhausts the nuclear fuel. As we mentioned previously, the gravitational collapse of the iron core cannot be hold by means of pressure heat from nuclear reactions. However, Chandrasekhar [3] showed that a total collapse can be avoided by the electronic pressure. In this situation, the core is stabilized due to the pressure of the degenerated electron gas,  $P(r)$ , and the inward gravitational pressure. This means that for a given point inside the star,

$$\begin{aligned} -\frac{Gm(r)}{r^2} \rho(r) &= \frac{dP(r)}{dr} = \frac{d\rho}{dr} \frac{dP}{d\rho}, \\ \frac{dm}{dr} &= 4\pi r^2 \rho(r), \\ \frac{dP}{d\rho} &= Y_e \frac{m_e}{M_N} \frac{x^2}{3\sqrt{1+x^2}}. \end{aligned} \tag{20}$$

where  $m_e$  and  $M_N$  are defined following Eq. 9.

This model is appropriate for a non-rotating white dwarf. With the boundary conditions  $m(r=0) = 0$  and  $\rho(r=0) = \rho_c$  (the central density), these equations can be solved easily [4]. For a given  $Y_e$ , the model is totally determined by  $\rho_c$ . Figure 4 shows the mass density of a white dwarf. We observe that the total mass of a white dwarf (of the order of a solar mass,  $M_\odot = 1.98 \times 10^{33}$  g), increases with  $\rho_c$ . Nonetheless, and perhaps the most important, it cannot exceed the finite value of

$$M \leq M_{Ch} \simeq 1.45 (2Y_e)^2 M_\odot, \tag{21}$$

which is know as the *Chandrasekhar mass* [3]. Applying these results to the nucleus of a star with any mass, we get from Eq. 20 that stars with mass  $M > M_{Ch}$  cannot be stable against the gravitational collapse by the pressure of the degenerate electron gas. The collapse occurs inevitably for a massive star, since the silicon burning adds more and more material to the stellar core.

At the beginning of the collapse the temperature and density are of the order of  $T \sim 10^{10}$  K and  $\rho \sim 3 \times 10^9$  g/cm<sup>3</sup>. The core is made of  $^{56}\text{Fe}$  and of electrons. There are two possibilities, both accelerating the collapse:

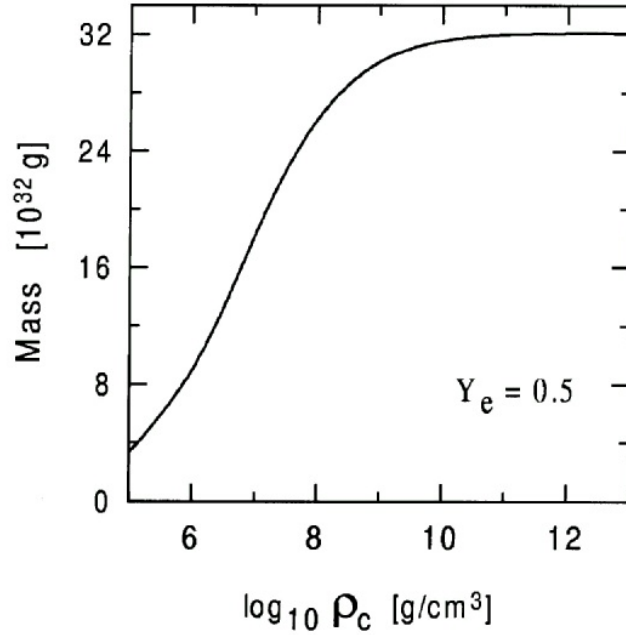


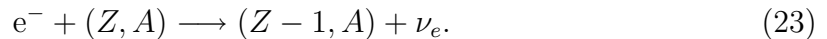
Figure 4: Masses of white dwarfs calculated as a function of  $\rho_c$ , the central density. With increasing  $\rho_c$ , the mass reaches a limiting value, the Chandrasekhar mass.

1. At conditions present in the collapse the strong reactions and the electromagnetic reactions between the nuclei are in equilibrium with their inverse, i.e.,



For example, with  $\rho = 3 \times 10^9 \text{ g/cm}^3$  and  $T = 11 \times 10^9 \text{ K}$ , half of  ${}^{56}\text{Fe}$  is dissociated. This dissociation takes energy from the core and causes pressure loss. The collapse is thus accelerated.

2. If the mass of the core exceeds  $M_{Ch}$ , electrons are captured by the nuclei to avoid the violation of the Pauli principle:



The neutrinos can escape the core, taking away energy. This is again accompanied by a pressure loss due to the decrease of the free electrons (this also decreases  $M_{Ch}$ ). The collapse is again accelerated.

The gravitational contraction increases the temperature and density of the core. An important change in the physics of the collapse occurs when the density reaches  $\rho_{\text{trap}} \simeq$

$4 \times 10^{11}$  g/cm<sup>3</sup>. The neutrinos become essentially confined to the core, since their diffusion time in the core is larger than the collapse time. After the neutrino confinement no energy is taken out of the core. Also, all reactions are in equilibrium, including the capture process 23. The degeneracy of the neutrino Fermi gas avoids a complete neutronization, directing the reaction 23 to the left. As a consequence,  $Y_e$  remains large during the collapse ( $Y_e \approx 0.3-0.4$  [5]). To equilibrate the charge, the number of protons must also be large. To reach  $Z/A = Y_e \approx 0,3-0,4$ , the protons must be inside heavy nuclei which will therefore survive the collapse.

Two consequence follows:

1. The pressure is given by the degenerate electron gas that controls the whole collapse; the collapse is thus adiabatic, with the important consequence that the collapse of the most internal part of the core is *homologous*, i.e., the position  $r(t)$  and the velocity  $v(t)$  of a given element of mass of the core are related by

$$r(t) = \alpha(t)r_0; \quad v(t) = \frac{\dot{\alpha}}{\alpha}r(t), \quad (24)$$

where  $r_0$  is the initial position.

2. Since the nuclei remain in the core of the star, the collapse has a reasonably large order and the entropy remains small during the collapse [5] ( $S \approx 1.5 k$  per nucleon, where  $k$  is the Boltzmann constant).

The collapse continues homologously until nuclear densities of the order of  $\rho_N \approx 10^{14}$  g/cm<sup>3</sup> are reached, when the matter can be thought as approximately a degenerate Fermi gas of nucleons. Since the nuclear matter has a finite compressibility, the homologous core decelerate and starts to increase again as a response to the increase of the nuclear matter. This eventually leads to a *shock wave* which propagates to the external core (i.e., the iron core outside the homologous core) which, during the collapse time, continued to contract reaching the supersonic velocity. The collapse break followed by the shock wave is the mechanism which breads the supernova explosion. Nonetheless, several ingredients of this scenario are still unknown, including the equation of state of the nuclear matter. The compressibility influences the available energy for the shock wave, which must be of the order of  $10^{51}$  erg.

The exact mechanism for the explosion of a supernova is still controversial.

1. In the *direct mechanism*, the shock wave is not only strong enough to stop the collapse, but also to explode the exterior stellar shells.
2. If the energy in the shock wave is insufficient for a direct explosion, the wave will deposit its energy in the exterior of the core, e.g., by excitation of the nuclei, what is frequently followed by electronic capture and emission of neutrinos (*neutrino eruption*).

Additionally, neutrinos of the all three species are generated by the production of pairs in the hot environment. A new shock wave can be generated by the outward diffusion of neutrinos, what indeed carries the most part of the energy liberated in the gravitational collapse of the core ( $\approx 10^{53}$  erg). If about 1% of the energy of the neutrinos is converted into kinetic energy due to the coherent neutrino-nucleus scattering, a new shock wave arises. This will be strong enough to explode the star. This process is know as the *retarded mechanism* for supernova explosion.

To know which of the above mechanism is responsible for the supernova explosion one needs to know the rate of electron capture, the nuclear compressibility, and the way neutrinos are transported. The iron core, remnant of the explosion (the homologous core and part of the external core) will not explode and will become either a neutron star, and possibly later a *pulsar* (rotating neutron star), or a *black-hole*, as in the case of more massive stars, with  $M \geq 25 - 35M_{\odot}$ .

Type-II supernovae are defined as those showing H-lines in their spectra. It is likely that most, if not all, of the exploding massive stars still have some H-envelope left, and thus exhibit such a feature. In contrast, Type-I supernovae lack H in their ejecta.

---

## Supplement A

---

## 0.2 Thermonuclear rates and reaction networks

### 0.2.1 Cross sections and reaction rates

The nuclear cross section for a reaction between target  $j$  and projectile  $k$  is defined by

$$\sigma = \frac{\text{number of reactions target}^{-1}\text{sec}^{-1}}{\text{flux of incoming projectiles}} = \frac{r/n_j}{n_k v}. \quad (25)$$

where the target number density is given by  $n_j$ , the projectile number density is given by  $n_k$ , and  $v$  is the relative velocity between target and projectile nuclei. Then  $r$ , the number of reactions per  $\text{cm}^3$  and sec, can be expressed as  $r = \sigma v n_j n_k$ , or, more generally,

$$r_{j,k} = \int \sigma |v_j - v_k| d^3 n_j d^3 n_k. \quad (26)$$

The evaluation of this integral depends on the type of particles and distributions which are involved. For nuclei  $j$  and  $k$  in an astrophysical plasma, obeying a Maxwell-Boltzmann distribution,

$$d^3 n_j = n_j \left(\frac{m_j}{2\pi kT}\right)^{3/2} \exp\left(-\frac{m_j^2 v_j^2}{2kT}\right) d^3 v_j, \quad (27)$$

## 0.2. THERMONUCLEAR RATES AND REACTION NETWORKS

---

Eq. 26 simplifies to  $r_{j,k} = \langle \sigma v \rangle n_j n_k$ , where  $\langle \sigma v \rangle$  is the average of  $\sigma v$  over the temperature distribution in 27. More specifically,

$$r_{j,k} = \langle \sigma v \rangle_{j,k} n_j n_k \quad (28)$$

$$\langle j, k \rangle \equiv \langle \sigma v \rangle_{j,k} = \left(\frac{8}{\mu\pi}\right)^{1/2} (kT)^{-3/2} \int_0^\infty E \sigma(E) \exp(-E/kT) dE. \quad (29)$$

Here  $\mu$  denotes the reduced mass of the target-projectile system. In astrophysical plasmas with high densities and/or low temperatures, effects of electron screening become highly important. This means that the reacting nuclei, due to the background of electrons and nuclei, feel a different Coulomb repulsion than in the case of bare nuclei. Under most conditions (with non-vanishing temperatures) the generalized reaction rate integral can be separated into the traditional expression without screening 28 and a *screening factor* [6]

$$\langle j, k \rangle^* = f_{scr}(Z_j, Z_k, \rho, T, Y_i) \langle j, k \rangle. \quad (30)$$

This screening factor is dependent on the charge of the involved particles, the density, temperature, and the composition of the plasma. Here  $Y_i$  denotes the abundance of nucleus  $i$  defined by  $Y_i = n_i/(\rho N_A)$ , where  $n_i$  is the number density of nuclei per unit volume and  $N_A$  Avogadro's number. At high densities and low temperatures screening factors can enhance reactions by many orders of magnitude and lead to *pynonuclear ignition*.

When in Eq. 26 particle  $k$  is a photon, the relative velocity is always  $c$  and quantities in the integral are not dependent on  $d^3 n_j$ . Thus it simplifies to  $r_j = \lambda_{j,\gamma} n_j$  and  $\lambda_{j,\gamma}$  results from an integration of the photodisintegration cross section over a Planck distribution for photons of temperature  $T$

$$d^3 n_\gamma = \frac{1}{\pi^2 (c\hbar)^3} \frac{E_\gamma^2}{\exp(E_\gamma/kT) - 1} dE_\gamma \quad (31)$$

$$r_j = \lambda_{j,\gamma}(T) n_j = \frac{1}{\pi^2 (c\hbar)^3} \int d^3 n_j \int_0^\infty \frac{c\sigma(E_\gamma) E_\gamma^2}{\exp(E_\gamma/kT) - 1} dE_\gamma. \quad (32)$$

There is, however, no direct need to evaluate photodisintegration cross sections, because, due to detailed balance, they can be expressed by the capture cross sections for the inverse reaction  $l + m \rightarrow j + \gamma$  [7]

$$\lambda_{j,\gamma}(T) = \left(\frac{G_l G_m}{G_j}\right) \left(\frac{A_l A_m}{A_j}\right)^{3/2} \left(\frac{m_u kT}{2\pi\hbar^2}\right)^{3/2} \langle l, m \rangle \exp(-Q_{lm}/kT). \quad (33)$$

This expression depends on the reaction Q-value  $Q_{lm}$ , the temperature  $T$ , the inverse reaction rate  $\langle l, m \rangle$ , the partition functions  $G(T) = \sum_i (2J_i + 1) \exp(-E_i/kT)$  and the mass numbers  $A$  of the participating nuclei in a thermal bath of temperature  $T$ .

A procedure similar to Eq. 32 is used for electron captures by nuclei. Because the electron is about 2000 times less massive than a nucleon, the velocity of the nucleus  $j$  is negligible in the center of mass system in comparison to the electron velocity ( $|v_j - v_e| \approx |v_e|$ ). The electron capture cross section has to be integrated over a Boltzmann, partially degenerate, or Fermi distribution of electrons, dependent on the astrophysical conditions. The electron capture rates are a function of  $T$  and  $n_e = Y_e \rho N_A$ , the electron number density [8]. In a neutral, completely ionized plasma, the electron abundance is equal to the total proton abundance in nuclei  $Y_e = \sum_i Z_i Y_i$  and

$$r_j = \lambda_{j,e}(T, \rho Y_e) n_j. \quad (34a)$$

This treatment can be generalized for the capture of positrons, which are in a thermal equilibrium with photons, electrons, and nuclei. At high densities ( $\rho > 10^{12} \text{gcm}^{-3}$ ) the size of the neutrino scattering cross section on nuclei and electrons ensures that enough scattering events occur to thermalize a neutrino distribution. Then also the inverse process to electron capture (neutrino capture) can occur and the neutrino capture rate can be expressed similarly to Eqs. 32 or 34a, integrating over the neutrino distribution. Also inelastic neutrino scattering on nuclei can be expressed in this form. Finally, for normal decays, like beta or alpha decays with half-life  $\tau_{1/2}$ , we obtain an equation similar to Eqs.32 or 34a with a decay constant  $\lambda_j = \ln 2 / \tau_{1/2}$  and

$$r_j = \lambda_j n_j. \quad (35)$$

The nuclear cross section for charged particles is strongly suppressed at low energies due to the Coulomb barrier. For particles having energies less than the height of the Coulomb barrier, the product of the penetration factor and the MB distribution function at a given temperature results in the so-called *Gamow peak*, in which most of the reactions will take place. Location and width of the Gamow peak depend on the charges of projectile and target, and on the temperature of the interacting plasma (see Fig. 5).

Experimentally, it is more convenient to work with the astrophysical  $S$  factor

$$S(E) = \sigma(E) E \exp(2\pi\eta), \quad (36)$$

with  $\eta$  being the Sommerfeld parameter, describing the s-wave barrier penetration  $\eta = Z_1 Z_2 e^2 / \hbar v$ . In this case, the steep increase of the cross section is transformed in a rather flat energy dependent function (see Fig. 6). One can easily see the two contributions of the velocity distribution and the penetrability in the integral

$$\langle \sigma v \rangle = \left( \frac{8}{\pi \mu} \right)^{1/2} \frac{1}{(kT)^{3/2}} \int_0^\infty S(E) \exp \left[ -\frac{E}{kT} - \frac{b}{E^{1/2}} \right], \quad (37)$$

where the quantity  $b = 2\pi\eta E^{1/2} = (2\mu)^{1/2} \pi e^2 Z_j Z_k / \hbar$  arises from the barrier penetrability. Experimentally it is very difficult to take direct measurements of fusion reactions involving charged

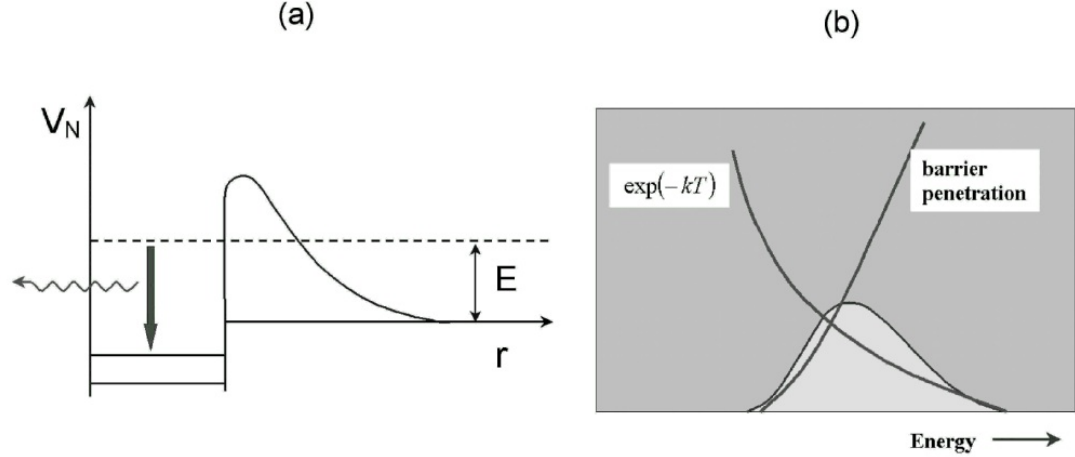


Figure 5: (a) Schematic representation of the nuclear+Coulomb potential for fusion of charged particles. (b) The integrand of eq. 29 is the product of an exponentially falling distribution with a fast growing cross section in energy.

particles at very small energies. The experimental data can be guided by a theoretical model for the cross section, which can then be extrapolated to the Gamow energy, as displayed in Fig. 6(b). The dots symbolize the experimental data points. The solid curve is a theoretical prediction, which supposedly describes the data. Its extrapolation to lower energies yields the desired value of the S-factor (and of  $\sigma$ ) at the energy  $E_0$ . The extrapolation can be inadequate due to the presence of resonances and of subthreshold resonances, as shown schematically in the figure.

Taking the first derivative of the integrand in Eq. 37 yields the location  $E_0$  of the Gamow peak, and the effective width  $\Delta$  of the energy window can be derived accordingly

$$\begin{aligned}
 E_0 &= \left( \frac{bkT}{2} \right)^{2/3} = 1.22(Z_j^2 Z_k^2 AT_6^2)^{1/3} \text{ keV}, \\
 \Delta &= \frac{16E_0 kT^{1/2}}{3} = 0.749(Z_j^2 Z_k^2 AT_6^5)^{1/6} \text{ keV},
 \end{aligned} \tag{38}$$

as shown in [10], carrying the dependence on the charges  $Z_j$ ,  $Z_k$ , the reduced mass  $A$  of the involved nuclei in units of  $m_u$ , and the temperature  $T_6$  given in  $10^6$  K. In Supplement A we show how one can get extended analytical results for the effective S-factor for non-resonant reactions.

In the case of neutron-induced reactions the effective energy window has to be derived in a slightly different way. For s-wave neutrons ( $l = 0$ ) the energy window is simply given by the location and width of the peak of the MB distribution function. For higher partial waves the penetrability of the centrifugal barrier shifts the effective energy  $E_0$  to higher energies. For neutrons with energies

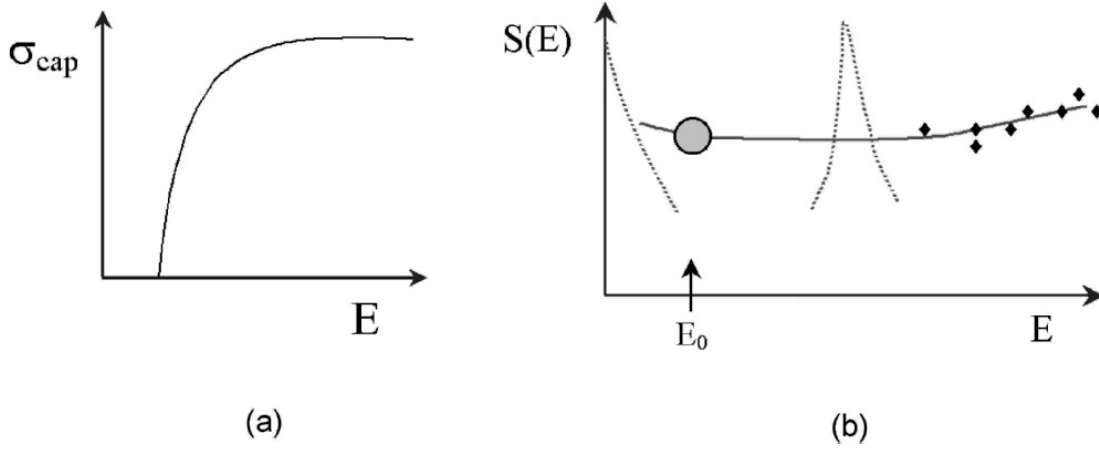


Figure 6: a) Schematic representation of the energy dependence of a fusion reaction involving charged particles. (b) The astrophysical S-factor as defined by eq. 36.

less than the height of the centrifugal barrier this was approximated by [9]

$$E_0 \approx 0.172T_9 \left( l + \frac{1}{2} \right) \text{ MeV}, \quad \Delta \approx 0.194T_9 \left( l + \frac{1}{2} \right)^{1/2} \text{ MeV. keV}, \quad (39)$$

The energy  $E_0$  will always be comparatively close to the neutron separation energy.

## 0.2.2 Reaction networks

The time derivative of the number densities of each of the species in an astrophysical plasma (at constant density) is governed by the different expressions for  $r$ , the number of reactions per  $\text{cm}^3$  and sec, as discussed above for the different reaction mechanisms which can change nuclear abundances

$$\left( \frac{\partial n_i}{\partial t} \right)_{\rho=\text{const}} = \sum_j N_j^i r_j + \sum_{j,k} N_{j,k}^i r_{j,k} + \sum_{j,k,l} N_{j,k,l}^i r_{j,k,l}. \quad (40)$$

The reactions listed on the right hand side of the equation belong to the three categories of reactions: (1) decays, photodisintegrations, electron and positron captures and neutrino induced reactions ( $r_j = \lambda_j n_j$ ), (2) two-particle reactions ( $r_{j,k} = \langle j, k \rangle n_j n_k$ ), and (3) three-particle reactions ( $r_{j,k,l} = \langle j, k, l \rangle n_j n_k n_l$ ) like the triple-alpha process ( $\alpha + \alpha + \alpha \rightarrow {}^{12}\text{C} + \gamma$ ), which can be interpreted as successive captures with an intermediate unstable target ( $\alpha + {}^8\text{Be}^* \rightarrow {}^{12}\text{C} + \gamma$ ). The individual  $N_i^i$ 's are given by:  $N_j^i = N_i$ ,  $N_{j,k}^i = N_i / \prod_{m=1}^{n_m} |N_{j_m}|!$ , and  $N_{j,k,l}^i = N_i / \prod_{m=1}^{n_m} |N_{j_m}|!$ . The  $N_i^i$ 's can be positive or negative numbers and specify how many particles of species  $i$  are created or destroyed in a reaction. The denominators, including factorials, run

over the  $n_m$  different species destroyed in the reaction and avoid double counting of the number of reactions when identical particles react with each other (for example in the  $^{12}\text{C}+^{12}\text{C}$  or the triple-alpha reaction) [7]. In order to exclude changes in the number densities  $\dot{n}_i$ , which are only due to expansion or contraction of the gas, the nuclear abundances  $Y_i = n_i/(\rho N_A)$  were introduced. For a nucleus with atomic weight  $A_i$ ,  $A_i Y_i$  represents the mass fraction of this nucleus, therefore  $\sum A_i Y_i = 1$ . In terms of nuclear abundances  $Y_i$ , a reaction network is described by the following set of differential equations

$$\dot{Y}_i = \sum_j N_j^i \lambda_j Y_j + \sum_{j,k} N_{j,k}^i \rho N_A \langle j, k \rangle Y_j Y_k + \sum_{j,k,l} N_{j,k,l}^i \rho^2 N_A^2 \langle j, k, l \rangle Y_j Y_k Y_l. \quad (41)$$

Eq. 41 derives directly from Eq. 40 when the definition for the,  $Y_i$ 's is introduced. This set of differential equations is solved numerically. They can be rewritten as difference equations of the form  $\Delta Y_i / \Delta t = f_i(Y_j(t + \Delta t))$ , where  $Y_i(t + \Delta t) = Y_i(t) + \Delta Y_i$ . In this treatment, all quantities on the right hand side are evaluated at time  $t + \Delta t$ . This results in a set of non-linear equations for the new abundances  $Y_i(t + \Delta t)$ , which can be solved using a multi-dimensional *Newton-Raphson iteration procedure*. The total energy generation per gram, due to nuclear reactions in a time step  $\Delta t$  which changed the abundances by  $\Delta Y_i$ , is expressed in terms of the mass excess  $M_{ex,i} c^2$  of the participating nuclei

$$\Delta \epsilon = - \sum_i \Delta Y_i N_A M_{ex,i} c^2, \quad \dot{\epsilon} = - \sum_i \dot{Y}_i N_A M_{ex,i} c^2. \quad (42a)$$

Therefore, the important ingredients to nucleosynthesis calculations are decay half-lives, electron and positron capture rates, photodisintegrations, neutrino induced reaction rates, and strong interaction cross sections.

---

### 0.3 Thermonuclear reaction rates: Models

Explosive nuclear burning in astrophysical environments produces unstable nuclei, which again can be targets for subsequent reactions. In addition, it involves a very large number of stable nuclei, which are not fully explored by experiments. Thus, it is necessary to be able to predict reaction cross sections and thermonuclear rates with the aid of theoretical models. Especially during the hydrostatic burning stages of stars, charged-particle induced reactions proceed at such low energies that a direct cross-section measurement is often not possible with existing techniques. Hence extrapolations down to the stellar energies of the cross sections measured at the lowest possible energies in the laboratory are the usual procedures to apply. To be trustworthy, such extrapolations should have as strong a theoretical foundation as possible. Theory is even more mandatory when excited nuclei are involved in the entrance channel, or when unstable very neutron-rich or neutron-deficient nuclides (many of them

being even impossible to produce with present-day experimental techniques) have to be considered. Such situations are often encountered in the modelling of explosive astrophysical scenarios.

Various models have been developed in order to complement the experimental information.

(a) Microscopic models. In this model, the nucleons are grouped into clusters. Keeping the internal cluster degrees of freedom fixed, the totally antisymmetrized relative wave functions between the various clusters are determined by solving the Schrödinger equation for a many-body Hamiltonian with an effective nucleon-nucleon interaction. When compared with most others, this approach has the major advantage of providing a consistent, unified and successful description of the bound, resonant, and scattering states of a nuclear system. Various improvements of the model have been made ([11]).

The microscopic model has been applied to many important reactions involving light systems, and in particular to the various p-p chain reactions ([13]). The available experimental data can generally be well reproduced. The microscopic cluster model or its variant (the microscopic potential model) has also made an important contribution to the understanding of the key  $^{12}\text{C}(\alpha, \gamma)^{16}\text{O}$  reaction rate ([12]).

(b) The potential and DWBA models. The potential model has been known for a long time to be a useful tool in the description of radiative capture reactions. It assumes that the physically important degrees of freedom are the relative motion between the (structureless) fragment nuclei in the entrance and exit channels, and that the fragments themselves are just accounted for approximately by the introduction of spectroscopic factors and strength factors in the optical potential. The associated drawbacks are that the nucleus-nucleus potentials adopted for calculating the initial and final wave functions from the Schrödinger equation cannot be unambiguously defined, and that the spectroscopic factors cannot be derived from first principles. They have instead to be obtained from more or less rough “educated guesses.”

The potential model has been applied, for example, to the p-p chain  $^3\text{He}(\alpha, \gamma)^7\text{Be}$  reaction [11], to the  $^7\text{Be}(p, \gamma)^8\text{B}$  [14], and to the  $^8\text{Li}(n, \gamma)^9\text{Li}$  [15] reactions.

(c) Parameter fits. Reaction rates dominated by the contributions from a few resonant or bound states are often extrapolated in terms of *R*- or *K*-matrix fits, which rely on quite similar strategies. The appeal of these methods rests on the fact that analytical expressions which allow for a rather simple parametrization of the data can be derived from underlying formal reaction theories. However, the link between the parameters of the *R*-matrix model and the experimental data (resonance energies and widths) is only quite indirect. The *K*-matrix formalism solves this problem, but suffers from other drawbacks ([16]).

The *R*- and *K*-matrix models have been applied to a variety of reactions, and in particular to the analysis of the  $^{12}\text{C}(\alpha, \gamma)^{16}\text{O}$  reaction rate ([17]).

(d) The statistical models. Many astrophysical scenarios involve a wealth of reactions on intermediate-mass or heavy nuclei. This concerns the non-explosive or explosive burning of

C, Ne, O and Si, as well as the s-, r- and p-process nucleosynthesis. Fortunately, a large fraction of the reactions of interest proceed through compound systems that exhibit high enough level densities for statistical methods to provide a reliable description of the reaction mechanism. In this respect, the *Hauser-Feshbach (HF) model* has been widely used with considerable success. Explosive burning in supernovae involves in general intermediate mass and heavy nuclei. Due to a large nucleon number they have intrinsically a high density of excited states. A high level density in the compound nucleus at the appropriate excitation energy allows to make use of the statistical model approach for compound nuclear reactions [18] which averages over resonances.

A high level density in the compound nucleus permits to use averaged transmission coefficients  $T$ , which do not reflect a resonance behavior, but rather describe absorption via an imaginary part in the (optical) nucleon-nucleus potential as described in Ref. [19]. This leads to the well known expression

$$\begin{aligned} \sigma_i^{\mu\nu}(j, o; E_{ij}) &= \frac{\pi \hbar^2 / (2\mu_{ij} E_{ij})}{(2J_i^\mu + 1)(2J_j + 1)} \\ &\times \sum_{J, \pi} (2J + 1) \frac{T_j^\mu(E, J, \pi, E_i^\mu, J_i^\mu, \pi_i^\mu) T_o^\nu(E, J, \pi, E_m^\nu, J_m^\nu, \pi_m^\nu)}{T_{tot}(E, J, \pi)} \end{aligned} \quad (43)$$

for the reaction  $i^\mu(j, o)m^\nu$  from the target state  $i^\mu$  to the excited state  $m^\nu$  of the final nucleus, with a center of mass energy  $E_{ij}$  and reduced mass  $\mu_{ij}$ .  $J$  denotes the spin,  $E$  the corresponding excitation energy in the compound nucleus, and  $\pi$  the parity of excited states. When these properties are used without subscripts they describe the compound nucleus, subscripts refer to states of the participating nuclei in the reaction  $i^\mu(j, o)m^\nu$  and superscripts indicate the specific excited states. Experiments measure  $\sum_\nu \sigma_i^{0\nu}(j, o; E_{ij})$ , summed over all excited states of the final nucleus, with the target in the ground state. Target states  $\mu$  in an astrophysical plasma are thermally populated and the astrophysical cross section  $\sigma_i^*(j, o)$  is given by

$$\sigma_i^*(j, o; E_{ij}) = \frac{\sum_\mu (2J_i^\mu + 1) \exp(-E_i^\mu/kT) \sum_\nu \sigma_i^{\mu\nu}(j, o; E_{ij})}{\sum_\mu (2J_i^\mu + 1) \exp(-E_i^\mu/kT)}. \quad (44)$$

The summation over  $\nu$  replaces  $T_o^\nu(E, J, \pi)$  in Eq.43 by the total transmission coefficient

$$\begin{aligned} T_o(E, J, \pi) &= \sum_{\nu=0}^{\nu_m} T_o^\nu(E, J, \pi, E_m^\nu, J_m^\nu, \pi_m^\nu) \\ &+ \int_{E_m^{\nu_m}}^{E-S_{m,o}} \sum_{J_m, \pi_m} T_o(E, J, \pi, E_m, J_m, \pi_m) \rho(E_m, J_m, \pi_m) dE_m. \end{aligned} \quad (45)$$

Here  $S_{m,o}$  is the channel separation energy, and the summation over excited states above the

highest experimentally known state  $\nu_m$  is changed to an integration over the level density  $\rho$ . The summation over target states  $\mu$  in Eq. 44 has to be generalized accordingly.

The important ingredients of statistical model calculations as indicated in the above equations are the particle and gamma-transmission coefficients  $T$  and the level density of excited states  $\rho$ . Therefore, the reliability of such calculations is determined by the accuracy with which these components can be evaluated (often for unstable nuclei).

The gamma-transmission coefficients have to include the dominant gamma-transitions (E1 and M1) in the calculation of the total photon width. The smaller, and therefore less important, M1 transitions have usually been treated with the simple single particle approach  $T \propto E^3$  of [20]. The E1 transitions are usually calculated on the basis of the Lorentzian representation of the Giant Dipole Resonance (see Supplement E). Within this model, the E1 transmission coefficient for the transition emitting a photon of energy  $E_\gamma$  in a nucleus  ${}^A_Z X$  is given by

$$T_{E1}(E_\gamma) = \frac{8}{3} \frac{NZ}{A} \frac{e^2}{\hbar c} \frac{1 + \chi}{mc^2} \sum_{i=1}^2 \frac{i}{3} \frac{\Gamma_{G,i} E_\gamma^4}{(E_\gamma^2 - E_{G,i}^2)^2 + \Gamma_{G,i}^2 E_\gamma^2}. \quad (46)$$

Here  $\chi (= 0.2)$  accounts for the neutron-proton exchange contribution, and the summation over  $i$  includes two terms which correspond to the split of the GDR in statically deformed nuclei, with oscillations along ( $i=1$ ) and perpendicular ( $i=2$ ) to the axis of rotational symmetry.

---

## Supplement B

---

### 0.4 The effective S-factor for a non-resonant reaction

In this supplement we show derivation of the effective S-factors  $S_{eff}$  for non-resonant reactions.

#### 0.4.1 Reaction rate and astrophysical S-factor

The reaction rate in the mixed gas of nuclei 1 and 2 is given by

$$R_{12} = \frac{1}{1 + \delta_{12}} N_1 N_2 \langle \sigma(E) v \rangle, \quad (47)$$

where  $N_i$ ,  $\sigma(E)$  and  $v$  are the number density of nucleus  $i$  ( $i = 1, 2$ ), the reaction cross section for the collision between nuclei 1 and 2 at the bombarding energy ( in the center of mass ) of  $E$

#### 0.4. THE EFFECTIVE S-FACTOR FOR A NON-RESONANT REACTION

---

and the relative velocity between the nuclei 1 and 2, respectively.  $\langle A \rangle$  is the average value over the Maxwell-Boltzmann distribution

$$\langle A \rangle = \left( \frac{\mu}{2\pi k_B T} \right)^{3/2} \int d^3v A \exp[-\mu v^2/2k_B T], \quad (48)$$

where  $\mu$ ,  $k_B$  and  $T$  are the reduced mass  $M_1 M_2 / (M_1 + M_2)$ , Boltzmann's constant and the temperature of the mixed gas, respectively.  $\delta_{12}$  avoids double-counting for the case of identical particles. Transforming the variable in Eq. 47 from  $v$  to  $E$  using a relationship  $E = \mu v^2/2$ , one obtains

$$R_{12} = \frac{N_1 N_2}{1 + \delta_{12}} \left( \frac{8}{\pi \mu} \right)^{1/2} \left( \frac{1}{k_B T} \right)^{3/2} \int_0^\infty dE S(E) \exp \left[ - \left( \frac{E}{k_B T} + 2\pi \eta(E) \right) \right], \quad (49)$$

where  $\eta(E)$  is the Sommerfeld parameter given by  $\eta(E) = Z_1 Z_2 e^2 / \hbar v$ , where  $Z_i$  is the atomic number of the nucleus  $i$ . On deriving Eq. 49 we employed the astrophysical S-factor, which is defined as in Eq. 36. In nuclear collisions at energies much lower than the Coulomb barrier, main energy dependences are  $1/E$  and  $\exp[-2\pi\eta(E)]$ . They are attributed to the geometrical cross section of a nucleus and the penetrability through the Coulomb barrier, respectively. Thus the energy dependence of the astrophysical S-factor results from the nuclear structure effects and for non-resonant reactions has a very weak energy-dependence.

In general, the nuclear reaction cross section at energies corresponding to the stellar interior temperature ( e.g., temperature in the central region of the Sun is about a few keV  $\approx 10^7$  K. ) is too small to measure using accelerators. One needs to extrapolate from data at high energies (  $\sim$  a few  $10^2$  keV ) to such a low energy region. In some cases the energy dependence of the astrophysical S-factor can be important to calculate the thermonuclear reaction rate.

Furthermore, due to developments of experimental techniques, experimental data with much better accuracy are now provided. At the same time one starts to consider that the weak dependence of S-factor on the energy should be taken into account. Formulae derived in this supplement are useful for such cases.

Using new variable  $x = E/k_B T$  and parameter

$$a = \left[ \pi \sqrt{2\mu} \frac{Z_1 Z_2 e^2}{\hbar} \right] \frac{1}{\sqrt{k_B T}} = \frac{b}{\sqrt{k_B T}} \quad ( > 0 ), \quad (50)$$

Eq. 49 is rewritten as

$$R_{12} = \frac{N_1 N_2}{1 + \delta_{12}} \left( \frac{8}{\pi \mu k_B T} \right)^{1/2} \int_0^\infty dx S(x k_B T) \exp \left[ - \left( x + \frac{a}{\sqrt{x}} \right) \right]. \quad (51)$$

In the next subsection we evaluate the integral 51 by using a conventional stationary phase approximation.

## 0.4.2 Gamow peak energy

On evaluation of Eq. 51, it is useful to introduce the Gamow peak energy  $E_0$  and  $\tau = 3E_0/k_B T$ . They are calculated in the conventional stationary phase approximation.

The phase of exponential in Eq. 51,

$$g(x) = x + \frac{a}{\sqrt{x}}, \quad (52)$$

behaves like a parabolic function with a positive curvature. Based on the concept of the stationary phase approximation, we suppose that only a narrow range around the stationary phase position

$$\begin{aligned} \left. \frac{dg(x)}{dx} \right|_{x=x_0} &= 1 - \frac{a}{2} x_0^{-3/2} = 0 \\ x_0 &= \left( \frac{a}{2} \right)^{2/3} \end{aligned} \quad (53)$$

contributes to the integration 51.  $g(x)$  may be able to be expanded as a Taylor power series in  $x$  around  $x_0$  up to the second order (Since  $g(x)$  behaves like a quadratic function)

$$g(x) \approx g(x_0) + \frac{1}{2} g''(x_0)(x - x_0)^2, \quad (54)$$

where  $g''(x)$  is the second derivative of  $g(x)$  with respect to  $x$ . Eq. 51 is then approximated to

$$\begin{aligned} R_{12} &\approx \frac{N_1 N_2}{1 + \delta_{12}} \left( \frac{8}{\pi \mu k_B T} \right)^{1/2} S(x_0 k_B T) \int_0^\infty \exp \left[ - \left( g(x_0) + \frac{g''(x_0)}{2} (x - x_0)^2 \right) \right] dx \\ &= \frac{N_1 N_2}{1 + \delta_{12}} \left( \frac{8}{\pi \mu k_B T} \right)^{1/2} S(x_0 k_B T) \exp[-g(x_0)] \left\{ \frac{2\pi}{g''(x_0)} \right\}^{1/2}. \end{aligned} \quad (55)$$

The Gamow peak energy  $E_0$  corresponds to the stationary phase position  $x_0$  through

$$E_0 = x_0 k_B T. \quad (56)$$

$g(x_0)$  and  $g''(x_0)$  are given by

$$\begin{aligned} g(x_0) &= x_0 + \frac{a}{\sqrt{x_0}} = \left( \frac{a}{2} \right)^{2/3} + \left( 2 \cdot \frac{a}{2} \right) \left( \frac{a}{2} \right)^{-1/3} = 3 \left( \frac{a}{2} \right)^{2/3} = 3x_0 = \frac{3E_0}{k_B T} = \tau \\ g''(x_0) &= \frac{3a}{4} x_0^{-5/2} = \frac{3}{2} \left( \frac{a}{2} \right) \cdot \left( \frac{a}{2} \right)^{-5/3} = \frac{3}{2x_0} = \frac{9}{2\tau}, \end{aligned} \quad (57)$$

respectively, where we used Eq. 53. We reach an expression of the conventional formula of the thermonuclear reaction rate

$$R_{12} \approx \frac{1}{1 + \delta_{12}} N_1 N_2 \left( \frac{8}{\pi \mu k_B T} \right)^{1/2} S(E_0) \frac{2}{3} (\pi \tau)^{1/2} e^{-\tau}, \quad (58)$$

#### 0.4. THE EFFECTIVE S-FACTOR FOR A NON-RESONANT REACTION

---

where the Gamow peak energy corresponds to the stationary phase position ( the position of the minimum for  $g(x)$  ) and is given by

$$E_0 = x_0 k_B T = \left( \frac{b k_B T}{2} \right)^{\frac{2}{3}}. \quad (59)$$

On the other hand,  $\tau$  is the minimum value of  $g(x)$  and is given by

$$\tau = \frac{3E_0}{k_B T} = 3 \left( \frac{b}{2} \right)^{\frac{2}{3}} \cdot (k_B T)^{-\frac{1}{3}}. \quad (60)$$

Concerning the reaction rate expressed in Eq. 58, three corrections are and will be needed to treat future experimental data of nuclear reactions with great accuracy. One is for a weak but significant energy variation of the astrophysical S-factor. Another is for a significant error resulting from substituting a Gaussian form for the sharply peaked exponential in Eq. 54. The other is for effects of electron screening (See Ref. [26], for example). We consider only the first two corrections.

Now let us introduce the effective S-factor. From Eqs. 49 and 58,  $S(E_0)$  is expressed as

$$\begin{aligned} S(E_0) &\approx \left\{ \frac{2}{3} (\pi\tau)^{1/2} e^{-\tau} \right\}^{-1} \frac{1}{k_B T} \int_0^\infty dE S(E) \exp \left[ - \left( \frac{E}{k_B T} + 2\pi\eta(E) \right) \right] \\ &= \sqrt{\frac{\tau}{4\pi}} \frac{e^\tau}{E_0} \int_0^\infty dE S(E) \exp \left[ - \left( \frac{E}{k_B T} + 2\pi\eta(E) \right) \right]. \end{aligned} \quad (61)$$

The r.h.s. of Eq. 61 is defined as the effective S-factor.

#### 0.4.3 Evaluation of integration by uniform expansion

In this subsection we evaluate the effective S-factor

$$\begin{aligned} S_{eff} &\equiv \sqrt{\frac{\tau}{4\pi}} \frac{e^\tau}{E_0} \int_0^\infty dE S(E) \exp \left[ - \left( \frac{E}{k_B T} + 2\pi\eta(E) \right) \right] \\ &= \left\{ \frac{2}{3} (\pi\tau)^{1/2} e^{-\tau} \right\}^{-1} \int_0^\infty dx S(x k_B T) \exp \left[ - \left( x + \frac{a}{\sqrt{x}} \right) \right] \end{aligned} \quad (62)$$

taking into account a weak dependence of the astrophysical S-factor on the energy. Assuming that  $S(E)$  is an analytic function of  $E$ , one can expand it as a Taylor power series in  $E$  around  $E = 0$  and  $E = E_0$

$$\begin{aligned} S(E) &= \sum_{n=0}^{\infty} \frac{1}{n!} \left( \frac{d^n S}{dE^n} \Big|_{E=0} \right) E^n = \sum_{n=0}^{\infty} \frac{1}{n!} \left( \frac{d^n S}{dE^n} \Big|_{E=E_0} \right) (E - E_0)^n \\ &= \sum_{n=0}^{\infty} \frac{1}{n!} \left( \frac{d^n S}{dE^n} \Big|_{E=E_0} \right) \sum_{r=0}^n (-)^r \binom{n}{r} E_0^r E^{n-r}, \end{aligned} \quad (63)$$

respectively. Using the power series 63, one can write Eq. 62 in the form

$$S_{eff-MT} = \left\{ \frac{2}{3} (\pi\tau)^{1/2} e^{-\tau} \right\}^{-1} \sum_{n=0}^{\infty} \frac{(k_B T)^n}{n!} \left( \frac{d^n S}{dE^n} \Big|_{E=0} \right) f_n(a) \quad (64)$$

$$S_{eff-MS} = \left\{ \frac{2}{3} (\pi\tau)^{1/2} e^{-\tau} \right\}^{-1} \sum_{n=0}^{\infty} \frac{(k_B T)^n}{n!} \left( \frac{d^n S}{dE^n} \Big|_{E=0} \right) \sum_{r=0}^n (-)^r \binom{n}{r} x_0^r f_{n-r}(a),$$

respectively, where

$$f_n(a) = \int_0^{\infty} dx x^n \exp \left[ - \left( x + \frac{a}{\sqrt{x}} \right) \right]. \quad (65)$$

Using a new variable  $u \equiv x^{n+1}$ , Eq. 65 is transformed to

$$f_n(a) = \frac{1}{n+1} \int_0^{\infty} du e^{-H_n(a,u)} \quad \text{with} \quad H_n(a,u) = u^{\frac{1}{n+1}} + au^{-\frac{1}{2(n+1)}}. \quad (66)$$

In order to evaluate the integration 66, we employ the uniform approximation. Since the phase in Eq. 66,  $H_n(a,u)$ , behaves like a parabolic function with a positive curvature, we may be able to perform a mapping  $u \rightarrow t$  which satisfies

$$H_n(a, u(t)) = t^2 + A(a) \quad (67)$$

$$u(t = -\infty) = 0, \quad u(t = \infty) = \infty, \quad \frac{du}{dt} > 0. \quad (68)$$

The integration 66 thus reduces to

$$f_n(a) = \frac{1}{n+1} e^{-A} \int_{-\infty}^{\infty} dt \left( \frac{du}{dt} \right) e^{-t^2}. \quad (69)$$

$du/dt$  can be also expanded as a Taylor power series in  $t$  around the stationary phase position for  $t^2 + A(a)$ , i.e.  $t = 0$ , and is written as

$$\frac{du}{dt} = \sum_{k=0}^{\infty} \frac{t^k}{k!} \left( \frac{d^{k+1}u}{dt^{k+1}} \Big|_{t=0} \right). \quad (70)$$

The integration 69 is then described by

$$\begin{aligned} f_n(a) &= \frac{e^{-A}}{n+1} \sum_{k=0}^{\infty} \frac{1}{k!} \left( \frac{d^{k+1}u}{dt^{k+1}} \Big|_{t=0} \right) \int_{-\infty}^{\infty} dt t^k e^{-t^2} \\ &= \frac{2e^{-A}}{n+1} \sum_{k=0}^{\infty} \frac{1}{(2k)!} \left( \frac{d^{2k+1}u}{dt^{2k+1}} \Big|_{t=0} \right) \int_0^{\infty} dt t^{2k} e^{-t^2} \\ &= \frac{\sqrt{\pi} e^{-A}}{n+1} \sum_{k=0}^{\infty} \frac{1}{2^{2k}} \frac{1}{k!} \left( \frac{d^{2k+1}u}{dt^{2k+1}} \Big|_{t=0} \right), \end{aligned} \quad (71)$$

#### 0.4. THE EFFECTIVE S-FACTOR FOR A NON-RESONANT REACTION

---

where we used the formula

$$\int_0^\infty dx e^{-ax^2} x^{2n} = \frac{(2n-1)!!}{2^{n+1}} \sqrt{\frac{\pi}{a^{2n+1}}}. \quad (72)$$

We calculate the stationary phase position defined as

$$\left. \frac{\partial H_n(a, u)}{\partial u} \right|_{u=u_n} = 0, \quad (73)$$

to begin with. The  $k$ th-order derivative of  $H_n(a, u)$  with respect to  $u$  is written in the form

$$\begin{aligned} H_n^{(k)}(a, u) &= \frac{\partial^k H_n(a, u)}{\partial u^k} \\ &= u^{\frac{1}{n+1}-k} \left\{ C_k(n) + a(-)^k D_k(n) u^{-\frac{3}{2(n+2)}} \right\} \quad (k \geq 1) \end{aligned} \quad (74)$$

$$C_k(n) = \prod_{j=1}^k \left( \frac{1}{n+1} - (j-1) \right) \quad (k \geq 1) \quad (75)$$

$$D_k(n) = \prod_{j=1}^k \left( \frac{1}{2(n+1)} + (j-1) \right) \quad (k \geq 1). \quad (76)$$

Using Eqs. 74 – 76,  $H_n^{(1)}(a, u)$  is given by

$$\begin{aligned} H_n^{(1)}(a, u) &= u^{-\frac{n}{n+1}} \left\{ \frac{1}{n+1} - \frac{a}{2(n+1)} u^{-\frac{3}{2(n+1)}} \right\} \\ &= u^{-\frac{n}{n+1}} \frac{1}{n+1} \left\{ 1 - \frac{a}{2} u^{-\frac{3}{2(n+1)}} \right\}. \end{aligned} \quad (77)$$

The stationary phase position  $u_n$  is then given by

$$u_n = \left( \frac{a}{2} \right)^{\frac{2(n+1)}{3}} = \left( \frac{\tau}{3} \right)^{n+1}. \quad (78)$$

One can also obtain the following relationship from Eq. 78

$$a = 2 \left( \frac{\tau}{3} \right)^{\frac{3}{2}}. \quad (79)$$

Since  $u_n = u(t=0)$  (the property of the mapping  $u \rightarrow t$ ),  $A(a)$  in Eq. 71 is calculated by

$$A = H_n(a, u(t=0)) = H_n(a, u_n). \quad (80)$$

---

0.4. THE EFFECTIVE S-FACTOR FOR A NON-RESONANT REACTION

---

Substituting Eqs. 78 and 79 into Eq. 80, one can write  $A(a)$  as

$$\begin{aligned} A(a) &= H_n(a, u_n) = \left(u^{\frac{1}{n+1}}\right) + 2 \left(\frac{\tau}{3}\right)^{\frac{3}{2}} \left(u^{\frac{1}{n+1}}\right)^{-1/2} \\ &= \left(\frac{\tau}{3}\right) + 2 \left(\frac{\tau}{3}\right)^{\frac{3}{2}} \left(\frac{\tau}{3}\right)^{-1/2} = \tau. \end{aligned} \quad (81)$$

Substituting Eqs. 78 and 79 into Eq. 74, one obtains the following expression

$$H_k = H_n^{(k)}(a, u_n) = \left(\frac{\tau}{3}\right)^{1-k(n+1)} \{C_k(n) + 2(-)^k D_k(n)\}. \quad (82)$$

Using Eq. 82,  $H_n^{(2)}(a, u_n)$  is expressed by

$$\begin{aligned} H_2 &= H_n^{(2)}(a, u_n) = \left(\frac{\tau}{3}\right)^{-(2n+1)} \left\{ \frac{1}{n+1} \left(\frac{1}{n+1} - 1\right) + \frac{1}{(n+1)} \left(\frac{1}{2(n+1)} + 1\right) \right\} \\ &= \left(\frac{\tau}{3}\right)^{-(2n+1)} \frac{3}{2(n+1)^2}. \end{aligned} \quad (83)$$

We here rewrite Eq. 71 so as to have similar a structure of Eq. 55

$$\begin{aligned} f_n(a) &= \frac{1}{n+1} \left\{ \frac{2\pi}{H_n^{(2)}(a, u_n)} \right\}^{1/2} \sqrt{\frac{H_n^{(2)}(a, u_n)}{2}} e^{-H_n(a, u_n)} \\ &\quad \times \sum_{k=0}^{\infty} \frac{1}{2^{2k}} \frac{1}{k!} \left( \left. \frac{d^{2k+1}u}{dt^{2k+1}} \right|_{t=0} \right) \\ &= \frac{1}{n+1} \left\{ 2\pi \frac{2(n+1)^2}{3} \frac{\tau}{3} \left(\frac{\tau}{3}\right)^{2n} \right\}^{1/2} e^{-\tau} \sqrt{\frac{H_n^{(2)}(a, u_n)}{2}} \\ &\quad \times \sum_{k=0}^{\infty} \frac{1}{2^{2k}} \frac{1}{k!} \left( \left. \frac{d^{2k+1}u}{dt^{2k+1}} \right|_{t=0} \right) \\ &= \frac{2}{3} (\pi\tau)^{1/2} e^{-\tau} \left(\frac{\tau}{3}\right)^n \sum_{k=0}^{\infty} Q_{2k}(u_n[\tau]), \end{aligned} \quad (84)$$

where

$$Q_{2k}(u_n[\tau]) = \frac{1}{2^{2k}} \frac{1}{k!} \sqrt{\frac{H_n^{(2)}(a, u_n)}{2}} \left( \left. \frac{d^{2k+1}u}{dt^{2k+1}} \right|_{t=0} \right). \quad (85)$$

#### 0.4.4 Calculation of $Q_{2k}(u_n[\tau])$

In this subsection we will show how to calculate  $Q_{2k}(u_n)$ , i.e. how to derive the  $k$ th-order derivative of  $u(t)$  at  $t = 0$ . However, it is so elaborated that we will present the derivation of only the first term of  $Q_{2k}(u_n)$ .

Firstly, one differentiates Eq. 67 with respect to  $t$ . Noted that we don't write the parameter  $a$  in  $H_n$  explicitly in the following.

$$\frac{dH_n(u(t))}{dt} = \frac{dH_n(u)}{du} \cdot \frac{du}{dt} = 2t. \quad (86)$$

If one substitutes  $u_n$  and  $t = 0$  into Eq. 86, both r.h.s and l.h.s in Eq. 86 vanish so that one cannot obtain  $du(t=0)/dt$ . Thus, differentiating furthermore Eq. 86 with respect to  $t$ , one obtains

$$\frac{d^2 H_n}{du^2} \left( \frac{du}{dt} \right)^2 + \frac{dH_n}{du} \left( \frac{d^2 u}{dt^2} \right) = 2 \quad (87)$$

and

$$\left( \frac{du}{dt} \Big|_{t=0} \right) = \sqrt{\frac{2}{H_n^{(2)}(u_n)}}. \quad (88)$$

From Eqs. 85 and 88, one can find easily

$$Q_0(u_n) = 1. \quad (89)$$

Repeating such differentiations,  $d^k u(t=0)/dt^k$  is expressed by a multinomial of  $H_n^{(k)}(u_n)$ . Fortunately, Ref. [27] provides the multinomial for  $Q_k(u_n)$  up to  $k = 10$ . We here show them in case of  $k = 2, 4$  and  $6$

$$\begin{aligned} Q_2(u_n) &= \frac{1}{24H_2^3} (5H_3^2 - 3H_2H_4) \\ Q_4(u_n) &= \frac{1}{1152H_2^6} (385H_3^4 - 630H_2H_3^2H_4 + 105H_2^2H_4^2 + 168H_2^2H_3H_5 - 24H_2^3H_6) \\ Q_6(u_n) &= \frac{1}{414720H_2^{10}} (425425H_3^6 - 1126125H_2H_3^4H_4 + 675675H_2^2H_3^3H_4^2 \\ &\quad - 51975H_2^3H_4^3 + 360360H_2^2H_3^3H_5 - 249480H_2^3H_3H_4H_5 \\ &\quad + 13608H_2^4H_5^2 - 83160H_2^3H_3^2H_6 + 22680H_2^4H_4H_6 \\ &\quad + 12960H_2^4H_3H_7 - 1080H_2^5H_8), \end{aligned} \quad (90)$$

where

$$H_k = H_n^{(k)}(u_n). \quad (91)$$

---

0.4. THE EFFECTIVE S-FACTOR FOR A NON-RESONANT REACTION

---

Using Eqs. 82, 75 and 76, one can reduce the above expressions to the following simple ones [28]

$$\begin{aligned}
 Q_0(u_n(\tau)) &= 1 \\
 Q_2(u_n(\tau)) &= \frac{1}{12\tau} [12n^2 + 18n + 5] \\
 Q_4(u_n(\tau)) &= \frac{1}{2! (12)^2 \tau^2} [144n^4 + 336n^3 + 84n^2 - 144n - 35] \\
 Q_6(u_n(\tau)) &= \frac{1}{3! (12)^3 \tau^3} [1728n^6 + 4320n^5 - 4320n^4 - 13320n^3 - 288n^2 \\
 &\quad + 6210n + 665] \\
 Q_{2k}(u_n(\tau)) &= \frac{1}{k! (12)^k \tau^k} P_{2k}(n), \tag{92}
 \end{aligned}$$

where  $P_{2k}(n)$  are polynomials of  $n$ . We can finally obtain the reaction rate formula for the non-resonant reaction

$$R_{12} = \frac{1}{1 + \delta_{12}} N_1 N_2 \left( \frac{8}{\pi \mu k_B T} \right)^{1/2} \frac{2}{3} (\pi \tau)^{1/2} e^{-\tau} S_{eff} \tag{93}$$

and two expressions of the effective S-factor

$$S_{eff-MT} = \sum_{n=0}^{\infty} \frac{1}{n!} E_0^n \left( \frac{d^n S}{dE^n} \Big|_{E=0} \right) \sum_{k=0}^{\infty} \frac{P_{2k}(n)}{k! (12)^k \tau^k} \tag{94}$$

$$S_{eff-MS} = \sum_{n=0}^{\infty} \frac{1}{n!} E \left( \frac{d^n S}{dE^n} \Big|_{E=0} \right) \sum_{r=0}^n (-)^r \binom{n}{r} \sum_{k=0}^{\infty} \frac{P_{2k}(n-r)}{k! (12)^k \tau^k} \tag{95}$$

with

$$\begin{aligned}
 P_0(n) &= 1 \\
 P_2(n) &= 12n^2 + 18n + 5 \\
 P_4(n) &= 144n^4 + 336n^3 + 84n^2 - 144n - 35 \\
 P_6(n) &= 1728n^6 + 4320n^5 - 4320n^4 - 13320n^3 - 288n^2 + 6210n + 665 \\
 P_{2k}(n) &= \dots\dots\dots \tag{96}
 \end{aligned}$$

High  $n$ th-derivative of  $S(E)$  and high- $k$  terms involving  $\tau^{-k}$  can be negligible practically so that one can set the maximum numbers of  $n$  and  $k$ ,  $n_M$  and  $k_N$ , respectively. For example, if one chooses  $n_M = 2$  and  $k_M = 1$ , one can obtain the same expression of Eq. (5) in Refs. [29] and [26].

An example of Eq. 94 in case of  $n_M = 5$  and  $k_M = 3$  is given in Ref. [28].

---

## 0.5 Role of exotic nuclei in nuclear astrophysics

### 0.5.1 Masses

Nuclear masses (equivalently, binding or separation energies) enter all chapters of nuclear astrophysics. Their knowledge is indispensable in order to evaluate the rate and the energetics of any nuclear transformation.

Figure ?? displays the approximately 2500 nuclides that have been identified by now in the laboratory. Among them, 286 are naturally occurring, the remaining ones being artificially produced. As extended as it is, this data set does not quite meet the astrophysics requirements. This is especially true when dealing with the r-process nucleosynthesis, which involves a large number of nuclei unidentified in the laboratory.

The development of radioactive beam facilities allows an increasing variety of proton- or neutron-rich nuclei to be studied, and this tendency will certainly develop further. The accuracy of the measurements is also significantly improving, and may now reach the 10 keV level, even for nuclei relatively far from the line of stability. Roughly speaking, these experiments involve high-precision direct mass measurements using high-resolution spectrometers, or indirect measurements based on the study of the energetics of a nuclear transformation from which an unknown mass can be deduced from the knowledge of the other participating nuclei. Despite the experimental advances, many masses remain to be measured in order to meet the astrophysics needs, so that recourse has to be made to theory.

### 0.5.2 Nuclei at high temperatures

The existence in a stellar plasma of nuclei in their ground as well as excited states has an important bearing on various decay modes or nuclear transmutations, and consequently on different nucleosynthesis processes. In many cases, therefore, the determination of the ground state mass is insufficient and the evaluation of “nuclear partition functions,” i.e. sums of the equilibrium populations of the states of a nucleus, has to be carried out. This is typically the case when abundances have to be evaluated in conditions where reactions and their reverses equilibrate. An extreme case of this situation is the “nuclear statistical equilibrium (NSE)” regime.

The fact that nuclear excited states enter various nuclear astrophysics calculations obviously makes indispensable the knowledge of nuclear spins and energies of these states. Such information is often missing experimentally, especially when dealing with “exotic” nuclei far from stability, or even with stable nuclei when high temperatures have to be considered. In such cases, relatively high-energy levels may indeed be significantly populated.

### 0.5.3 Nuclear decays and reactions via weak interaction

Weak interaction processes play a decisive role in a wide variety of astrophysical questions. A very specific example of the importance of weak interaction concerns the starting transmutation  $\text{H} + \text{H} \rightarrow {}^2\text{He} + e^+ + \nu_e$  of the p-p chain of reactions, which is the essential H-burning mode in the very large galactic population of stars with masses  $M \lesssim 1 M_\odot$ . In more advanced stages of evolution, various sorts of weak interaction processes occur, some of which are unknown in the laboratory, just as the H + H reaction.

Aside from the capture of continuum electrons on protons (and on iron-group nuclides), various weak-interaction processes involving neutrinos also have an important bearing on Type-II supernovae. The probabilities of production of all sorts of (anti-)neutrinos at the centre of a nascent (hot) neutron star, certain reaction cross sections that determine their transport rate to the neutron star surface, and the interactions of the emerging neutrinos with neutrons and protons near that surface are expected to be essential ingredients of the Type-II supernova models [30].

The excited levels and ground state of a nucleus are very often populated in thermal equilibrium, possible exceptions being certain isomeric states. These various levels may thus contribute to the decay of a nucleus, so that its effective  $\beta$ -decay half-life may strongly depart from the laboratory value.

The development of radioactive beam facilities and of highly efficient detectors has been quite beneficial. This is exemplified by the determination of the half-lives of the magic or near-magic nuclei  ${}^{130}\text{Cd}$ ,  ${}^{79}\text{Cu}$ , and of their neighbors taking part in the r-process [31]. The use of a very fast in-flight separation technique has led to the measurement of the  $\beta$ -decay properties of  ${}^{44}\text{S}$  and  ${}^{45-47}\text{Cl}$  [32], which are of astrophysical interest. The  $\beta$ -decay half-lives of neutron-rich Fe, Co, Ni and Cu isotopes of r-process relevance have also been obtained following their production by neutron-induced fission [33]. Measurements concerned with very neutron-rich nuclei have also been performed following their production in relativistic projectile fission [34] or in fragmentation reactions [35]. On the proton-rich side, experiments conducted at several facilities have helped clarifying the location of the proton drip line, and have provided an ensemble of  $\beta$ -decay rates of relevance to the rp- or  $\alpha$ p-processes [36].

### 0.5.4 Nuclear decays and reactions via electromagnetic interaction

Nuclei immersed in a high-temperature stellar photon bath may be subjected to photodisintegrations of the  $(\gamma, n)$ ,  $(\gamma, p)$  or  $(\gamma, \alpha)$  types. Because of the experimental (and theoretical) difficulties raised by the direct determination of photodisintegration rates, especially under the constraint that the photons obey a Planck distribution law, use is usually made of the detailed balance theorem applied to the reverse radiative captures of nucleons or  $\alpha$ -particles. This procedure makes clear that the photodisintegration rates depend on temperature  $T$

and on the reaction  $Q$ -value as  $\exp(-Q/kT)$ . The Coulomb dissociation method [?] with radioactive beams, to be discussed ahead, is an alternative method to probe some of the reactions needed.

### 0.5.5 Charged-particle induced reactions

Direct methods have been, and still are, widely utilized in the case of stable targets, all efforts being directed towards the development of techniques permitting to reach smaller and smaller cross sections and/or higher and higher accuracies. Typically, use is made of a dedicated accelerator delivering for several weeks low-energy ion beams of high intensity (1 mA) on a target that is able to withstand the heavy beam load (hundreds of watts), and that is also of high chemical and isotopic purity. A few per mil atoms of impurity can indeed be responsible for a noise exceeding the expected signal. In the case of the commonly used inverse kinematics geometry, a heavy-ion accelerator is often used in conjunction with a windowless gas target of the static or supersonic jet type. New generations of detector systems and pulse-processing electronics that have primarily been developed for nuclear structure studies will certainly be most welcome in the attempt to measure sub-picobarn cross sections.

In the case of unstable targets, two different direct approaches are envisioned, depending upon the lifetimes of the nuclides involved in the entrance channel. The radioactive *target* technique appears most profitable for radio-active nuclides with lifetimes in excess of about one hour. It has been applied in particular to  $^{22}\text{Na}(p, \gamma)^{23}\text{Mg}$  and  $^{26}\text{Al}^g(p, \gamma)^{27}\text{Si}$ . In contrast, the radioactive *beam* method is appropriate for shorter-lived species, and has without doubt to be seen as a new frontier in nuclear physics and astrophysics. Two basic techniques can be used to produce the high-intensity, high-purity radioactive beams that are required for the study of the low-energy resonances or non-resonant contributions of astrophysical interest.

A major breakthrough is the direct use of medium-energy or relativistic radioactive ion beams from projectile fragmentation. As an example, this technique has been applied to the direct measurement of  $^8\text{Li}(\alpha, n)^{11}\text{B}$  [38], which has been predicted to be of interest in an inhomogeneous Big Bang model.

The indirect methods are a very important complement, or even an inevitable alternative, to the direct measurements concerning reactions on stable as well as unstable targets. This situation relates in particular to the extreme smallness of the cross sections of astrophysical interest, or to the incapability of setting up radioactive beams of the required purity and intensity.

Different indirect approaches have been developed and applied to a more or less large extent, like (1) the use of transfer reactions, (2) the study of the inverse reactions, or (3) measurements relating to the decay of radioactive beams. In cases where resonances near or below the reaction threshold can contribute significantly to the reaction rate, extrapolations of the rates from high energies to the Gamow window may fail. In such conditions, the

Breit–Wigner parameters (energy, angular momentum, partial and total widths, and decay modes) of the involved resonances must be determined independently. In nuclear structure studies, this information is typically obtained via transfer reactions. They are well suited for investigations using radioactive beams or targets.

### 0.5.6 Decay of radioactive beams

In certain cases, radioactive decays may offer an interesting alternative to transfer reactions for exploring nuclear levels of astrophysical importance. For example, the  $\beta$ -decay of  $^{20}\text{Mg}$  has been studied in order to improve the knowledge of the  $^{20}\text{Na}$  level structure above the  $^{19}\text{Na} + p$  threshold, and concomitantly of the  $^{19}\text{Ne}(p, \gamma)^{20}\text{Na}$  break-out reaction from the hot CNO cycle [41].

Similarly,  $^{12}\text{C}(\alpha, \gamma)^{16}\text{O}$  has been investigated through the  $\beta$ -delayed  $\alpha$ -emission from  $^{16}\text{N}$  [42] - [43], and through the  $\beta$ -delayed proton emission from  $^{17}\text{N}$  [44]. These experiments provide information on the E1 and E2 contributions to the rate, respectively.

---

## Supplement C

---

### 0.5.7 Neutrinos as solar thermometers

The Sun serves as a very important test case for a variety of problems related to stellar structure and evolution, as well as to fundamental physics. The central temperature  $T_{\odot}$  of the Sun is a nice example of a physical quantity which can be determined by means of solar neutrino detection, provided that the relevant nuclear physics is known (and neutrino properties are also known). Surprisingly enough for a star that has all reasons to be considered as one of the dullest astrophysical objects, the Sun has been for years at the centre of various controversies. One of them is the *solar neutrino problem*, referring to the fact that the pioneering  $^{37}\text{Cl}$  neutrino-capture experiments carried out over the years in the Homestake gold mine observe a neutrino flux that is substantially smaller than the one predicted by the solar models. That puzzle has led to a flurry of theoretical activities, and to the development of new detectors. These activities have transformed the original solar neutrino problem into problems. The relative levels of ‘responsibility’ of particle physics, nuclear physics or astrophysics in these discrepancies have been debated ever since. In Ref. [40], the discussion is conducted in particular in the light of the several experiment supporting the ideas of ‘oscillations’ between different neutrinos types [39]. In the neutrino oscillation picture, the electron-neutrino, detected by the chlorine experiment, can transform into a muon-neutrino on its way to the earth from the center of the Sun. This would explain the smaller number of electron-neutrinos observed at the earth.

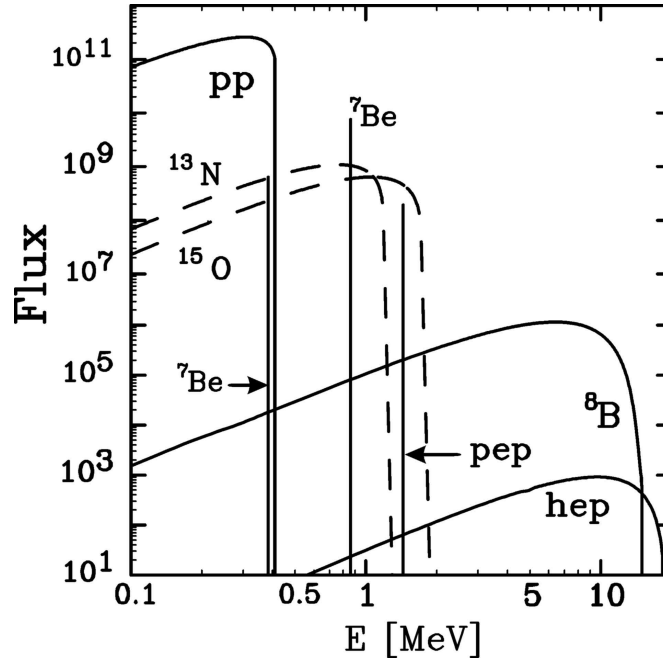


Figure 7: The solar neutrino spectrum, as calculated with the Standard Solar Model (SSM) [40].

SSM calculations [40] predict  $T_{\odot}$  with an accuracy of 1% or even better. In order to appreciate such a result, let us remind that the central temperature of Earth is known with an accuracy of about 20%. However, let us remind that this is a theoretical prediction which, as any result in physics, demands observational evidence.

The fluxes of  ${}^8\text{B}$  and  ${}^7\text{Be}$  neutrinos (see Fig. 1) are given by:

$$\Phi(B) = c_B S_{17} \frac{S_{34}}{\sqrt{S_{33}}} T_{\odot}^{20}, \quad \Phi(Be) = c_{Be} \frac{S_{34}}{\sqrt{S_{33}}} T_{\odot}^{10} \quad (97)$$

where  $S_{ij}$  are the low energy astrophysical factors for nuclear reactions between nuclei with atomic mass numbers  $i$  and  $j$ ,  $c_B$  and  $c_{Be}$  are well determined constants.

The high powers of  $T_{\odot}$  in the above equations imply that the measured neutrino fluxes are strongly sensitive to  $T_{\odot}$ , i.e.  ${}^7\text{Be}$  and  ${}^8\text{B}$  neutrinos in principle are good thermometers for the innermost part of the Sun. On the other hand, the relevant nuclear physics has to be known, which justifies the present theoretical and experimental efforts for better determinations of the  $S_{ij}$ .

Much experimental and theoretical work has been devoted to the reactions of the p-p chains that are the main energy and neutrino producers in the Sun. In spite of that, problems remain concerning the astrophysical rates of some of the involved reactions. This is especially the case for  ${}^7\text{Be}(p, \gamma){}^8\text{B}$  (which determines the value of  $S_{17}$  in Eq. 97), which provides the main neutrino

flux detectable by the chlorine detector, and is considered by some as one of the most important nuclear reactions for astrophysics. Improved low-energy data are also required for other reactions, like  ${}^3\text{He}({}^3\text{He},2\text{p}){}^4\text{He}$ . Since such low-energy measurements are predominantly hampered by the cosmic-ray background, improved data could be obtained by underground measurements.

---

## 0.6 Indirect methods

Nuclear capture reactions, such as  $(p, \gamma)$  and  $(\alpha, \gamma)$ , play a major role in defining our universe. A primary goal in nuclear astrophysics is to determine rates for capture reactions that are important in the evolution of stellar systems. However, the reactions of interest often involve radioactive targets which makes measurements quite difficult or even impossible using conventional methods. Hence techniques have been developed to determine rates by indirect methods. For example, precise information on excitation energies and particle decay widths can be used to make accurate predictions of rates which proceed by resonance capture. The only reliable method to determine a reaction rate that is dominated by direct capture has been to measure it at laboratory energies with a low energy particle beam and then extrapolate the result to energies of astrophysical interest.

### 0.6.1 Coulomb dissociation method

With increasing beam energy higher lying states of nuclei can be excited with the Coulomb excitation mechanism. This can lead to Coulomb dissociation, in addition to Coulomb excitation of particle bound states, for a review see , e.g., [45]. Such investigations are also well suited for secondary (radioactive) beams [37]. Due to the time-dependent electromagnetic field the projectile is excited to a bound or continuum state, which can subsequently decay. We briefly mention the very large effects of electromagnetic excitation in relativistic heavy ion collisions. If 1<sup>st</sup> order electromagnetic excitation is the dominant effect, experiments can directly be interpreted in terms of electromagnetic matrix elements, which also enter, e.g., in radiative capture cross-sections The question of higher order effects is therefore very important.

In the equivalent photon approximation the cross section for an electromagnetic process is written as

$$\sigma = \int \frac{d\omega}{\omega} n(\omega) \sigma_\gamma(\omega) \quad (98)$$

where  $\sigma_\gamma(\omega)$  denotes the appropriate cross section for the photo-induced process and  $n(\omega)$  is the equivalent photon number.

Since the equivalent photon numbers can be calculated theoretically, an experimental measurement of the Coulomb breakup reaction  $a + A \longrightarrow b + c + A$  is useful to obtain the

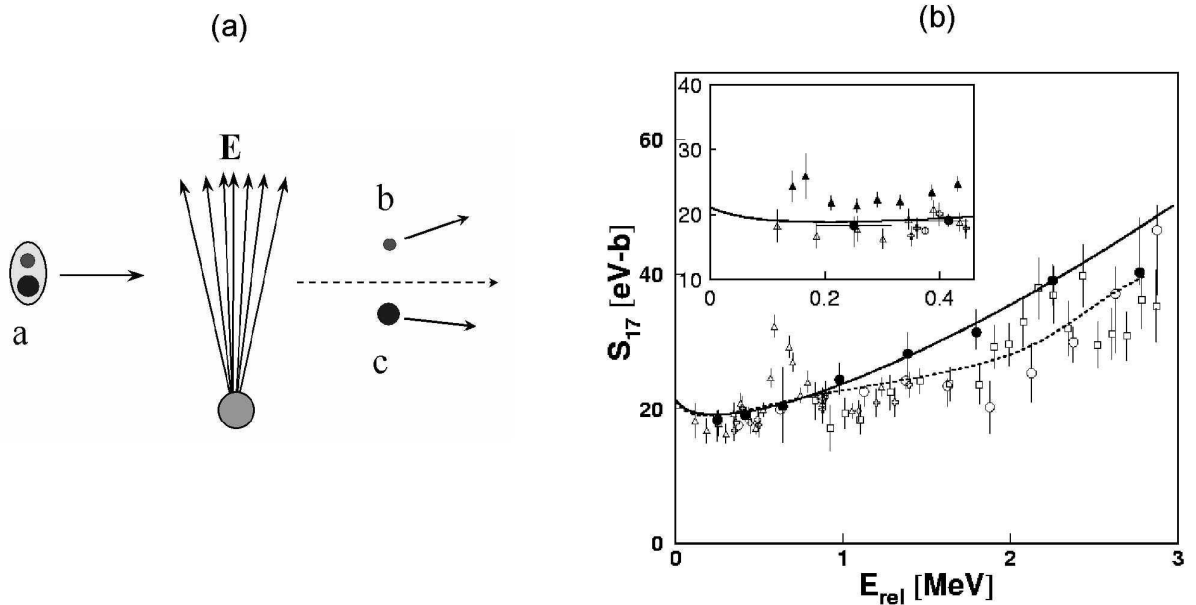


Figure 8: (a) The Coulomb dissociation method is based on the Coulomb breakup of a projectile in the electric field of a heavy nucleus. (b) World data for the astrophysical S-factor of the  ${}^7\text{Be}(p,\gamma){}^8\text{B}$  reaction [55], of relevance for understanding the energy production in the Sun. The solid data points were obtained with the Coulomb dissociation method [55]. The solid curve is a potential model calculation by Bertulani [14]. The dashed curve is a calculation by Descouvemont and Baye [56].

corresponding  $\gamma$ -induced cross section  $\gamma + a \rightarrow b + c$ . Using detailed balance, this cross section can be related to the radiative capture cross section  $b + c \rightarrow a + \gamma$ , of astrophysical interest [37]. In this case since  $\pi/k^2$  for a photon is approximately 100-1000 times larger than that of a particle beam, the small cross section is enhanced. The large virtual photon flux (typically 100-1000 photons per collision) also gives rise to enhancement of the cross section. However, the method is useful only when the higher order effects are under control, so that the Eq. 98, obtained in 1st-order perturbation theory, is valid. Higher order effects can be taken into account in a coupled channels approach, or by using higher order perturbation theory. The latter involves a sum over all intermediate states  $n$  considered to be important. Another approach is to integrate the time-dependent Schrödinger equation directly for a given model Hamiltonian [46, 47, 48, 49].

The method has been successfully applied, among others, to the important  ${}^{12}\text{C}(\alpha,\gamma){}^{16}\text{O}$  reaction [50]. With radioactive beams produced by the fragmentation of energetic heavy-ions, the Coulomb break-ups of  ${}^{14}\text{O}$ ,  ${}^{12}\text{N}$  and  ${}^8\text{B}$  have been used to study the reactions

$^{13}\text{N}(p,\gamma)^{14}\text{O}$  [51, 52],  $^{11}\text{C}(p,\gamma)^{12}\text{N}$  [53], and  $^7\text{Be}(p,\gamma)^8\text{B}$  [54, 55] (see Fig. 8 ).

The Coulomb dissociation can be a very useful tool to obtain information on  $(n,\gamma)$ -reaction cross sections on unstable nuclei, where direct measurements cannot be done, e.g., using nuclei like  $^{124}\text{Mo}$ ,  $^{126}\text{Ru}$ ,  $^{128}\text{Pd}$  and  $^{130}\text{Cd}$  as projectiles. The optimum choice of beam energy depends on the actual neutron binding energy. Since the flux of equivalent photons has essentially an  $1/\omega$  dependence, low neutron thresholds are favorable for the Coulomb dissociation method. Note that only information about the  $(n,\gamma)$  capture reaction to the ground state is possible with the Coulomb dissociation method.

It can also be applied to two nucleon capture reactions. Evidently, they cannot be studied in a direct way in the laboratory. Sometimes this is not necessary, when the relevant information about resonances involved can be obtained by other means (transfer reactions, etc.), like in the triple  $\alpha$ -process. Two-neutron capture reactions in supernovae neutrino bubbles are studied in Ref. [59]. In the case of a high neutron abundance, a sequence of two-neutron capture reactions,  $^4\text{He}(2n,\gamma)^6\text{He}(2n,\gamma)^8\text{He}$  can bridge the  $A = 5$  and 8 gaps. The  $^6\text{He}$  and  $^8\text{He}$  nuclei may be formed preferentially by two-step resonant processes through their broad  $2^+$  first excited states [59]. Another key reaction can be the  $^4\text{He}(\alpha n,\gamma)$  reaction [59].

In the rp-process, two-proton capture reactions can bridge the waiting points [57, 58, 60]. From the  $^{15}\text{O}(2p,\gamma)^{17}\text{Ne}$ ,  $^{18}\text{Ne}(2p,\gamma)^{20}\text{Mg}$  and  $^{38}\text{Ca}(2p,\gamma)^{40}\text{Ti}$  reactions considered in Ref. [58], the latter can act as an efficient reaction link at conditions typical for X-ray bursts on neutron stars. A  $^{40}\text{Ti} \rightarrow p + p + ^{38}\text{Ca}$ . The decay with two protons is expected to be sequential rather than correlated (“ $^2\text{He}$ ”-emission).

## 0.6.2 Asymptotic normalization coefficients

Direct capture reactions of astrophysical interest usually involve systems where the binding energy of the captured proton is low. Hence at stellar energies, the capture proceeds through the tail of the nuclear overlap wave function. The shape of this tail is completely determined by the Coulomb interaction, so the rate of the capture reaction can be calculated accurately if one knows its amplitude. The *asymptotic normalization coefficient (ANC)*  $C$  for the system  $B \leftrightarrow A + p$  specifies the amplitude of the single-proton tail of the wave function for nucleus  $B$  when the core  $A$  and the proton are separated by a distance large compared to the nuclear radius. Thus, this normalization coefficient determines the corresponding direct capture rate [61].

The advantage of the ANC approach is that it provides a method to determine direct capture S-factors accurately from the results of nuclear reactions such as peripheral nucleon transfer which can be studied with radioactive beams and have cross sections that are orders of magnitude larger than the direct capture reactions themselves. Furthermore, direct capture S-factors derived with this technique are most reliable at the lowest incident energies, precisely where capture cross sections are smallest and most difficult to measure directly. In

fact, the ANC approach even permits one to determine S-factors at zero energy, which is not possible with direct measurements except by extrapolation.

For a peripheral transfer reaction, ANC's are extracted from the measured angular distribution by comparison to a DWBA calculation. Consider the proton transfer reaction  $a + A \rightarrow c + B$ , where  $a = c + p$  and  $B = A + p$ . The experimental cross section is related to the DWBA calculation according to

$$\frac{d\sigma}{d\Omega} = \sum_{l_B j_B l_a j_a} (C_{Apl_B j_B}^B)^2 (C_{cpl_a j_a}^a)^2 R_{l_B j_B l_a j_a}, \quad (99)$$

where

$$R_{l_B j_B l_a j_a} = \frac{\tilde{\sigma}_{l_B j_B l_a j_a}}{b_{Apl_B j_B}^2 b_{cpl_a j_a}^2}. \quad (100)$$

$\tilde{\sigma}$  is the calculated DWBA cross section and the  $b$ 's are the asymptotic normalization constants for the single particle orbitals used in the DWBA. The sum in Eq. 99 is taken over the allowed angular momentum couplings, and the  $C$ 's are the ANC's for  $B \rightarrow A + p$  and  $a \rightarrow c + p$ . The normalization of the DWBA cross section by the ANC's for the single particle orbitals makes the extraction of the ANC for  $B \rightarrow A + p$  insensitive to the parameters used in the single particle potential wells [62], in contrast to traditional spectroscopic factors. See [62] for additional details.

The relation of the ANC's to the direct capture rate at low energies is straightforward [61]. The cross section for the direct capture reaction  $A + p \rightarrow B + \gamma$  can be written as

$$\sigma = \lambda | \langle I_{Ap}^B(\mathbf{r}) | \hat{O}(\mathbf{r}) | \psi_i^{(+)}(\mathbf{r}) \rangle |^2, \quad (101)$$

where  $\lambda$  contains kinematic factors,  $I_{Ap}^B$  is the overlap function for  $B \rightarrow A + p$ ,  $\hat{O}$  is the electromagnetic transition operator, and  $\psi_i^{(+)}$  is the incident scattering wave. If the dominant contribution to the matrix element comes from outside the nuclear radius, the overlap function may be replaced by

$$I_{Ap}^B(r) \approx C \frac{W_{-\eta, l+1/2}(2\kappa r)}{r}, \quad (102)$$

where  $C$  defines the amplitude of the tail of the radial overlap function  $I_{Ap}^B$ ,  $W$  is the Whittaker function,  $\eta$  is the Coulomb parameter for the bound state  $B = A + p$ , and  $\kappa$  is the bound state wave number. For example, in the case of  $^{16}\text{O}(p, \gamma)^{17}\text{F}$ , the necessary  $C$ 's are just the ANC's determined from the  $^{16}\text{O}(^3\text{He}, d)^{17}\text{F}$  transfer reaction studies [63]. Thus, the direct capture cross sections are directly proportional to the squares of these ANC's. In fact, the  $^{16}\text{O}(p, \gamma)^{17}\text{F}$  reaction populating the very weakly bound  $^{17}\text{F}$  first excited state provides an extreme test of the connection between the ANC measured in a transfer reaction and the S-factor measured in direct capture. The approximation of Eq. 102 is excellent at

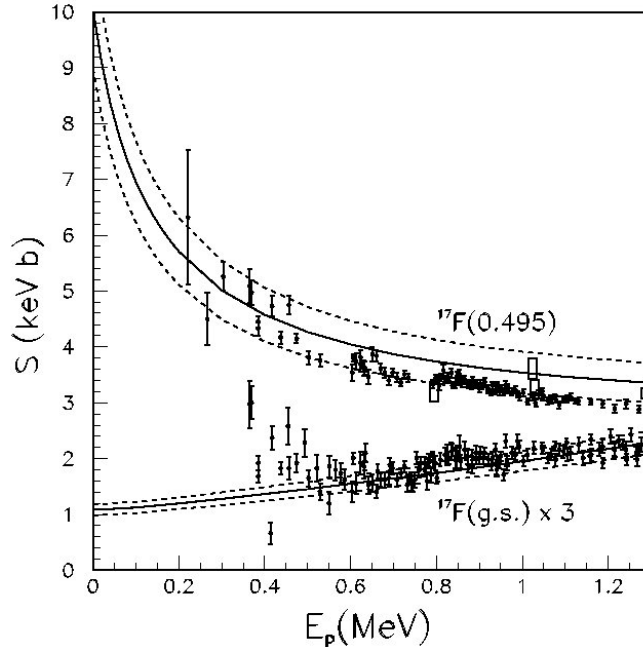


Figure 9: A comparison of the experimental S-factors to those determined from the ANC's found in  $^{16}\text{O}(^3\text{He}, d)^{17}\text{F}$ . The solid data points are from [64], and the open boxes are from [65]. The solid lines indicate our calculated S-factors, and the dashed lines indicate the  $\pm 1\sigma$  error bands. Note that the experimental ground state S-factor may be contaminated by background at energies below 500 keV.

large radii, but the proximity of the node in the  $2s_{1/2}$  wave function makes it rather poor near the nuclear surface. In contrast, Eq. 102 provides a good description of the  $^{17}\text{F}$  ground state  $1d_{5/2}$  wave function even in the vicinity of the nuclear surface.

Following the prescription outlined above, the S-factors for  $^{16}\text{O}(p, \gamma)^{17}\text{F}$  were calculated with no free parameters. The results are shown in Fig. 9.

Both  $E1$  and  $E2$  contributions have been included in the calculations, but the  $E1$  components dominate. The capture of protons by  $^{16}\text{O}$  at low energies occurs at very large distances  $r$  due to the extremely small proton separation energy of  $^{17}\text{F}$  [64]. Thus, one finds that the calculated capture cross sections are sensitive neither to the behavior of the overlap functions at small  $r$ , nor to the nuclear interaction between  $^{16}\text{O}$  and  $p$  in the initial state [65]. One finds that  $S(0) = 0.40 \pm 0.04$  keV·b for populating the  $^{17}\text{F}$  ground state and  $S(0) = 9.8 \pm 1.0$  keV·b for populating the first excited state. The uncertainties in these calculated zero-energy S-factors come almost entirely from those in the corresponding ANC's. There is no uncertainty associated with ambiguities in an extrapolation from higher incident energies

to zero energy, and there is very little theoretical uncertainty, since the capture reaction is almost purely peripheral at very low incident energies. In the astrophysical domain, the energy dependence of the capture cross sections is determined entirely by the initial Coulomb scattering wave functions and the kinematic factors, while their magnitudes are fixed by the ANC's. The theoretical uncertainty in the S-factors is less than 2% at an energy of 1 MeV, as estimated in Ref. [63]. Hence, the uncertainty in S at small energies is due just to the uncertainties in the ANC's. However, as the energy increases above 1 MeV, the calculated S-factors become more sensitive to the behavior of the overlap functions at smaller  $r$  and to the details of the nuclear interaction in the initial state. In that case, the simple direct radiative capture model used here breaks down, and a microscopic approach including antisymmetrization is needed. This effect has been studied for  ${}^7\text{Be}(p, \gamma){}^8\text{B}$  in [66].

Two previous measurements of  ${}^{16}\text{O}(p, \gamma){}^{17}\text{F}$  have determined the capture cross sections to the ground and first excited states separately [64, 65]. The experimental results for the S-factors populating the  ${}^{17}\text{F}$  ground and excited states are also shown in Fig. 9. It is clear from Fig. 9 that the agreement between the experimental results and the predictions based on the measured ANC's is indeed very good for proton energies below 1 MeV. At these energies, the  ${}^{16}\text{O}(p, \gamma){}^{17}\text{F}$  S-factors derived from the analysis of the  ${}^{16}\text{O}({}^3\text{He}, \text{d}){}^{17}\text{F}$  measurements [63] agree with the corresponding direct experimental results to better than 9%.

# Bibliography

- [1] J. N. Bahcall, *Neutrino Astrophysics*, Cambridge University Press, Cambridge, 1989.
- [2] I. Iben Jr., *Astrophys. J.* **41** (1965) 993.
- [3] S. Chandrasekhar, *Astrophys. J.* **74** (1931) 81; S. Chandrasekhar, *Rev. Mod. Phys.* **56** (1984) 137.
- [4] S. E. Koonin, *Computational Physics*, Addison-Wesley, Reading, Massachusetts, 1986.
- [5] H. A. Bethe, G. Brown, J. Applegate e J. M. Lattimer, *Nucl. Phys.* **A324** (1979) 487.
- [6] E.E. Salpeter, H.M. van Horn, *Ap. J.* **155** (1969) 183.
- [7] W. A. Fowler, G. E. Caughlan, B. A. Zimmermann, *Ann. Rev. Astron. Astrophys.* **5** (1967) 525.
- [8] G.M. Fuller, W.A. Fowler and M. Newman, *Ap. J.* **293** (1985) 1.
- [9] R.V. Wagoner, *Ap. J. Suppl.* **18** (1969) 247.
- [10] C. Rolfs, and W.S. Rodney, *Cauldrons in the Cosmos*, University of Chicago Press, Chicago, 1988.
- [11] P. Descouvemont, *Tours Symposium on Nuclear Physics III* [AIP Conf. Proc. **425**] (New York: Amer. Inst. Phys.), 1998, p. 418.
- [12] P. Descouvemont *Phys. Rev.* **C47** (1993) 210.
- [13] K. Langanke and C.A. Barnes, *Advances in Nuclear Physics* **22** Negele J W and Vogt E (eds) (New York: Plenum Press), 1996, p. 173.
- [14] C.A. Bertulani, *Z. Phys.* **A356** (1996) 293; C.A. Bertulani and M. Gai, *Nucl. Phys.* **A636** (1998) 227.
- [15] C.A. Bertulani, *J. Phys.* **G25** (1999) 1959.

- 
- [16] F.C. Barker, Nucl. Phys. **A575** (1994) 361.
- [17] R.E. Azuma *et al.*, Proc. *ENAM 95*, M. de Saint Simon and O. Sorlin (eds) (Gif-sur-Yvette: Editions Frontières),1995 , p. 619.
- [18] W. Hauser and H. Feshbach, Phys. Rev. **A87** (1952) 366.
- [19] C. Mahaux, H.A. Weidenmüller, Ann. Rev. Part. Nucl. Sci. **29** (1979) 1.
- [20] J.M. Blatt and H.F. Weisskopf, *Theoretical Nuclear Physics*, Wiley, New York,1952.
- [21] E.M. Burbidge *et al.*, Rev. Mod. Phys. **29** (1957) 547.
- [22] P.A. Seeger, W.A. Fowler and D.D. Clayton, Astrophys. J. Suppl. **11** (1965) 121.
- [23] S.Goriely, Phys. Lett. **B436** (1998) 10.
- [24] L. Van Wormer *et al.*, Astrophys. J. **432** (1994) 326.
- [25] H. Schatz *et al.*, Phys. Rep. **294** (1988)167.
- [26] E. G. Adelberger *et al.*, Rev. Mod. Phys. **70** (1998) 1265 .
- [27] R. B. Dingle, *Asymptotic Expansions: their derivation and interpretation*,New York & London Academic Press (1973).
- [28] M. S. Hussein and M. P. Pato, Braz. J. Phys. **27** (1997) 364.
- [29] B. K. Jennings and S. Karataglidis, Phys. Rev. **C58** (1998) 3002.
- [30] H.A. Bethe, Rev. Mod. Phys. **62** (1990) 801.
- [31] K.L. Kratz *et al.*,Z. Phys. **A340** (1991) 419.
- [32] O. Sorlin *et al.*, Phys. Rev. **C47** (1993) 2941.
- [33] M. Bernas *et al.*, Phys. Rev. Lett. **67** (1992) 3661.
- [34] M. Bernas *et al.*, Nucl. Phys. **A616** (1997) 352.
- [35] F. Ameil *et al.*, European Phys. J. **A1** (1998) 275.
- [36] E. Roeckl 1998 in *Proc. of the Hirschegg Workshop on Nuclear Astrophysics*, ed. by Buballa M *et al.* 1998, pp. 350.
- [37] G.Baur, C.A.Bertulani and H.Rebel, Nucl. Phys. **A458** (1986) 188.

- [38] X. Gu et al., Phys. Lett. **B343** (1995) 31.
- [39] Y. Fukuda et al., Phys. Rev. Lett. **81** (1998) 1158.
- [40] J.N. Bahcall, P.I. Krastev and Yu.A. Smirnov, Phys. Rev. **D58** (1998) 096016.
- [41] A. Piechaczek et al., *Radioactive Nuclear Beams III* (Gif-sur-Yvette: Editions Frontières) Morrisey D J (ed) 1993, p. 495.
- [42] R.E. Azuma et al., Phys. Rev. **C50** (1994) 1194.
- [43] Z. Zhao, R.H. France, K.S. Lai, S.L. Rugari, M. Gai, and E.L. Wilds, Phys. Rev. Lett. **70** (1993) 2066.
- [44] J.D. King et al., *Tours Symposium on Nuclear Physics III* [AIP Conf. Proc. **425**], ed. by Arnould M *et al.* (eds) 1998 (New York: Amer. Inst. Phys.), p. 372.
- [45] C. A. Bertulani and G. Baur, Phys. Rep. **163** (1988) 299.
- [46] H. Esbensen, G. F. Bertsch and C. A. Bertulani, Nucl. Phys. **A581** (1995) 107.
- [47] V. S. Melezhik and D. Baye, Phys. Rev. **C59** (1999) 3232.
- [48] H. Utsunomia, Y. Tokimoto, T. Yamagata, M. Ohta, Y. Aoki, K. Hirota, K. Ieki, Y. Iwata, K. Katori, S. Hamada, Y.-W. Lui, R. P. Schmitt, S. Typel and G. Baur, Nucl. Phys. **A654** (1999) 928c.
- [49] S. Typel, H. H. Wolter, Z. Naturforsch. **54a** (1999) 63.
- [50] V. Tatischeff et al., Phys. Rev. **C51** (1995) 2789.
- [51] T. Motobayashi et al., Phys. Lett. **B264** (1991) 259.
- [52] J. Kiener et al., Nucl. Phys. **A552** (1993) 66.
- [53] A. Lefebvre et al. Nucl. Phys. **A592** (1995) 69.
- [54] T. Motobayashi et al., Phys. Rev. Lett. **73** (1994) 2680.
- [55] N. Iwasa et al., Phys. Rev. Lett. **83** (1999) 2910.
- [56] P. Descouvemont and D. Baye, Nucl. Phys. **A567** (1994) 341.
- [57] *NuPECC Report, Nuclear and Particle Astrophysics*, July 16, 1997, I. Baraffe et al., F.-K. Thielemann (convener).

- 
- [58] J. Görres, M. Wiescher and F.-K. Thielemann, Phys. Rev. **C51** (1995) 392.
- [59] J. Görres, H. Herndl, I. J. Thompson and M. Wiescher, Phys. Rev. **C52** (1995) 2231.
- [60] H. Schatz et al., Phys. Rep. **294** (1998) 167.
- [61] H.M. Xu, C.A. Gagliardi, R.E. Tribble, A.M. Mukhamedzhanov, and N.K. Timofeyuk, Phys. Rev. Lett. **73** (1994) 2027.
- [62] C.A. Gagliardi, A.M. Mukhamedzhanov, R.E. Tribble, and H.M. Xu, Phys. Rev. Lett. **80**, 421 (1998).
- [63] C.A. Gagliardi et al., Phys.Rev. **C59** (1999) 1149.
- [64] R. Morlock, R. Kunz, A. Mayer, M. Jaeger, A. Muller, J.W. Hammer, P. Mohr, H. Oberhummer, G. Staudt, and V. Kolle, Phys. Rev. Lett. **79** (1997) 3837.
- [65] H.C. Chow, G.M. Griffith and T.H. Hall, Can. J. Phys. **53** (1975) 1672.
- [66] A. Csoto, Phys. Lett. B **394** (1997) 247.